View metadata, citation and similar papers at core.ac.uk

brought to you by CORE

provided by NASA Technical Reports Server

NASA/TP—1999–209267

Design and Test of Low-Profile Composite Aerospace Tank Dome

(MSFC Center Director's Discretionary Fund Final Report, Project No. 96–28)

R. Ahmed
Marshall Space Flight Center, Marshall Space Flight Center, Alabama

National Aeronautics and
Space Administration

Marshall Space Flight Center • MSFC, Alabama 35812

May 1999

Acknowledgments

The author gratefully acknowledges the efforts of the following people in the completion of this task:

- Derek Gefroh of University of Minnesota, NASA Academy Summer Student
- Robert Huff, Larry Pelham, and Gary Smith of Thiokol Corporation
- Marc Verhage, Steve Miller, and Chuck Wilkerson of NASA/MSFC.

A great many other people, whose names could not all be recalled by the author, worked to make this project a success. The author gratefully acknowledges their participation as well.

Available from:

NASA Center for AeroSpace Information
800 Elkridge Landing Road
Linthicum Heights, MD 21090–2934
(301) 621–0390

National Technical Information Service
5285 Port Royal Road
Springfield, VA 22161
(703) 487–4650

TABLE OF CONTENTS

LIST OF FIGURES

LIST OF FIGURES (Continued)

LIST OF FIGURES (Continued)

LIST OF TABLES

TECHNICAL PUBLICATION

DESIGN AND TEST OF LOW-PROFILE COMPOSITE AEROSPACE TANK DOME

(MSFC Center Director's Discretionary Fund Final Report, Project No. 96–28)

I. INTRODUCTION

In order to increase the structural performance of cryogenic tanks, the aerospace industry has begun to employ low-profile bulkheads in launch vehicle designs. A low-profile dome has a major-to-minor axis ratio greater than the square root of 2 and offers possibilities for maximizing the volume of a tank for a given length or for a shorter overall vehicle length for a given propellant volume. It can also minimize the length of interstage segments that join tanks together, thus contributing to a lower overall vehicle weight.

Previous studies have examined metallic aluminum alloy low-profile domes, but at the time of this writing limited work has been performed on low-profile domes constructed from composite materials. Composite materials offer the potential for further weight reduction over metallic materials due to the former's directional properties and higher strength-to-weight ratios. Consequently, a test project was initiated under the auspices of the Center Director's Discretionary Fund at the NASA Marshall Space Flight Center (MSFC) to validate the low-profile dome concept using a commonly used advanced aerospace composite material in a subscale ($\approx$1 m diameter) low-profile dome. This report describes the design, analysis, test, and results of this dome project.

A. Purpose

The objectives of the low-profile composite dome test were as follows:

1. Demonstrate the feasibility of low-profile composite dome designs.

2. Examine the structural response and failure modes for internally pressurized low-profile composite domes as a function of ply layup, number of plies (thickness), and a given fiber/matrix combination. The dome was appropriately instrumented to measure strain, displacement, and pressure under the applied loads. The data obtained from these tests would then be compared to analysis models and design guidelines for low-profile composite domes suggested.

B. Summary

This report presents the methodology behind the design of the low-profile composite dome, the means of its manufacture, the structural analysis that went into verifying the design before test, and the test itself. Test results (strains and displacements) are compared to the analysis predictions. Finally, assessments of the test article's strength and failure modes are given, along with suggestions for design of a low-profile composite dome.

II. LOW-PROFILE COMPOSITE DOME DESIGN AND MANUFACTURE

The low-profile composite dome was designed and manufactured during the spring and summer of 1996 (February through August) with the assistance of the Thiokol Corporation and the MSFC Productivity Enhancement Complex (PEC).

A. Design Principles for Low-Profile Composite Domes

To design a low-profile dome, it is necessary to have an understanding of the stress fields that occur in a vessel of revolution, which is created by rotating a two-dimensional shape about an axis through 360°.[1] The membrane stresses in such a vessel of revolution are axisymmetric; i.e., they are the same in any plane perpendicular to the axis of rotation. Figure 1 shows a generic shell of revolution and the stresses on a differential element. Only normal stresses act on this element.

The quantities in figure 1 are defined as follows:

σ_1 = stress in meridional direction

σ_2 = stress in hoop direction (direction along shell in circle perpendicular to axis of revolution)

r_1 = radius of curvature of element in meridional direction at a point

r_2 = radius of curvature of element in hoop direction at a point

ds_1 = element arc length in meridional direction

ds_2 = element arc length in hoop direction

$d\theta_1$ = angle swept by arc length in meridional direction

$d\theta_2$ = angle swept by arc length in hoop direction

h = thickness of shell

p = pressure applied (positive for internal pressure).

Applying equilibrium to the element in figure 1 gives:

$$2\sigma_2 h ds_1 \sin\left(\frac{d\theta_2}{2}\right) + 2\sigma_1 h ds_2 \sin\left(\frac{d\theta_2}{2}\right) = p\left(r_1 \sin d\theta_1 r_2 \sin d\theta_2\right) . \quad (1)$$

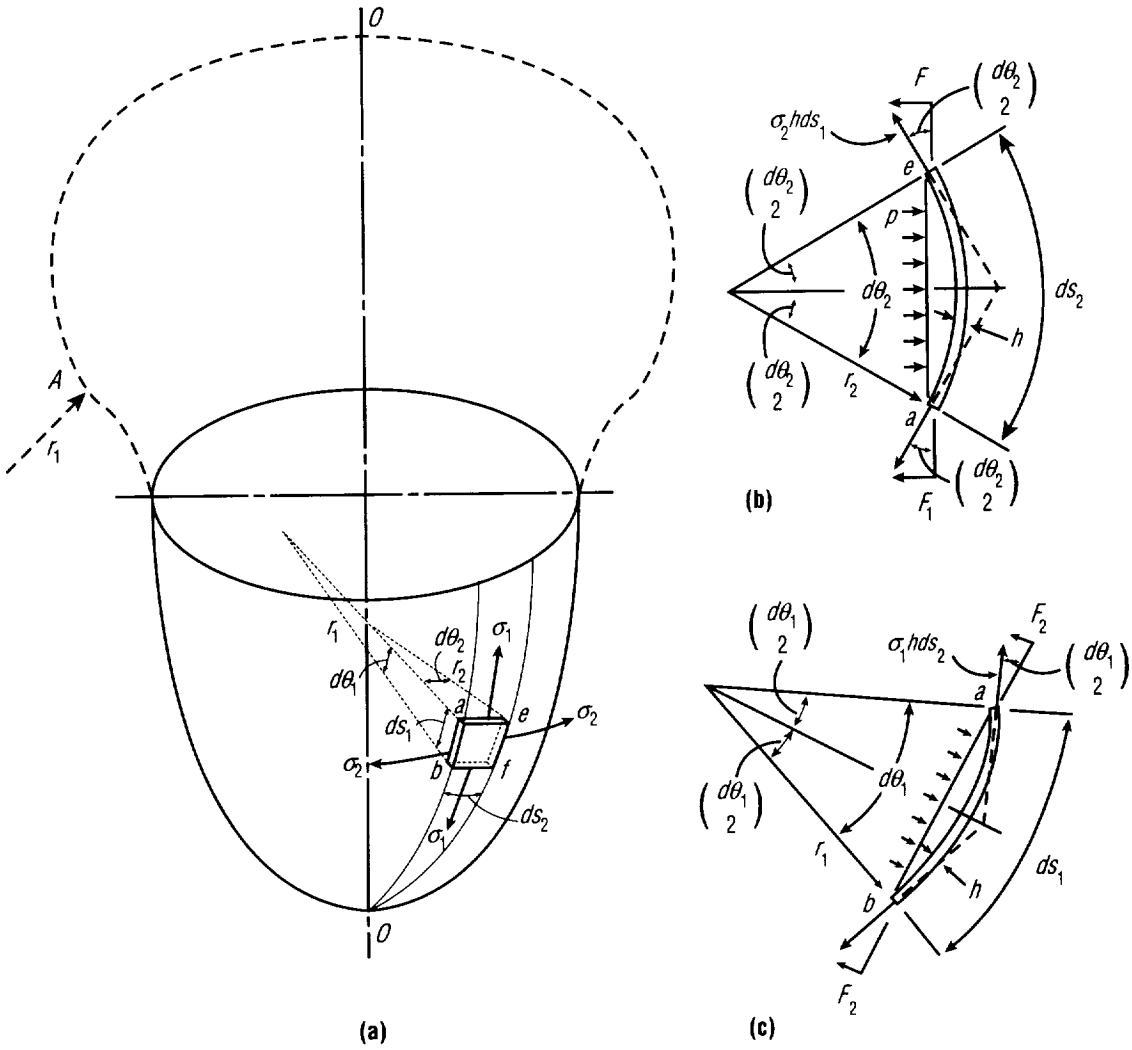

Figure 1. Stresses on a differential element in a generic shell of revolution.

Substituting $ds_1 = r_1 d\theta_1$ and $ds_2 = r_2 d\theta_2$ into (1) and noting that sin $d\theta = \theta$ for small angles yields the following:

$$\sigma_2 h r_1 + \sigma_1 h r_2 = p r_1 r_2 \ . \tag{2}$$

Rearranging (2) gives us:

$$\frac{\sigma_2}{r_2} + \frac{\sigma_1}{r_1} = p/h \ . \tag{3}$$

It is important to note again that r_1 is the local radius of curvature in the meridional direction, while r_2 is the radius of curvature in the hoop direction normal to the surface of the ellipsoid at a given point. r_1 is found using the curvature relation from elementary calculus and the equation of an ellipse as follows:

$$r_1 = \rho = \frac{\left[1+y'^2\right]^{3/2}}{y''} \quad , \tag{4}$$

and

$$\frac{x^2}{a^2} + \frac{y^2}{b^2} = 1 \quad , \tag{5}$$

where y' is the first derivative of y with respect to x, y'' is the second derivative of y with respect to x, and a and b are the major and minor axes, respectively, of the ellipse.

Rearranging (5) gives:

$$y = \left(\frac{b}{a}\right)\left(a^2 - x^2\right)^{1/2} \quad . \tag{6}$$

Finding y′ and y″ from (6) yields:

$$y' = -\frac{\frac{b}{a}x}{\left(a^2-x^2\right)^{1/2}} = -\left(\frac{b}{a}\right)^2 \frac{x}{y} \tag{7}$$

$$y'' = -\frac{b^4}{a^2 y^3} \quad . \tag{8}$$

Substituting (7) and (8) into (4) brings forth the following expression:

$$r_1 = \frac{\left[a^4y^2+b^4x^2\right]^{3/2}}{a^4b^4} \quad . \tag{9}$$

To find r_2, the normal to the surface is used as shown in figure 2. Defining l as the vertical component of r_2:

$$r_2 = \left[l^2+x^2\right]^{1/2} \quad . \tag{10}$$

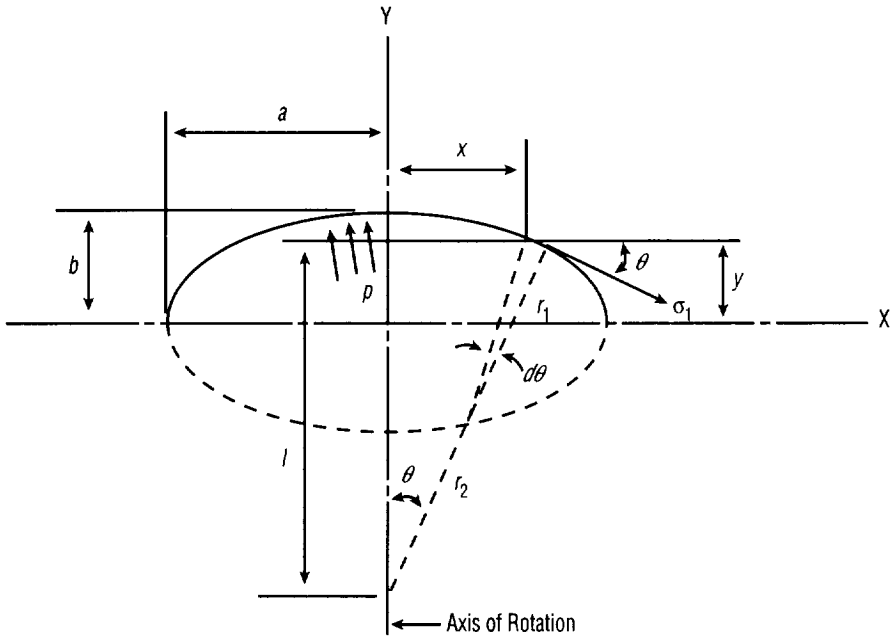

Figure 2. Definition of normals for calculating stress field in elliptical shell.

Noting that $\tan\theta = x/l = y'$ yields the following:

$$r_2 = \left[l^2\left(l+y'^2\right)\right]^{1/2} \tag{11}$$

with

$$l = \frac{x}{y'} = \frac{a^2 y}{b^2} = \left(\frac{a}{b}\right)\left[a^2 - x^2\right]^{1/2} \quad . \tag{12}$$

Substituting (7) and (12) into (11):

$$r_2 = \frac{\left[a^4 y^2 + x^2 b^4\right]^{1/2}}{b^2} \quad . \tag{13}$$

Taking the ratio of r_1 and r_2 gives:

$$r_1 = \left(\frac{b^2}{a^4}\right) {r_2}^3 \quad . \tag{14}$$

Now, applying equilibrium equations to a cut as shown in figure 2:

$$p\pi x^2 - \sigma_1(2\pi x)h\sin\theta = 0 \quad , \tag{15}$$

with

$$\sin\theta = \frac{x}{r_2} \quad . \tag{16}$$

Substituting (16) into (15) and rearranging gives:

$$\sigma_1 = \frac{pr_2}{2h} \quad . \tag{17}$$

Substituting (17) into (3):

$$\sigma_2 = \frac{pr_2}{2h}\left(2 - \frac{r_2}{r_1}\right) \quad , \tag{18}$$

remembering that σ_1 is the meridional stress and σ_2 is the hoop stress.

A summary of the key equations for computing stresses in low-profile domes follows:

Equation (6) $$y = \left(\frac{b}{a}\right)\left(a^2 - x^2\right)^{1/2}$$

Equation (9) $$r_1 = \frac{\left[a^4y^2 + b^4x^2\right]^{3/2}}{a^4b^4}$$

Equation (13) $$r_2 = \frac{\left[a^4y^2 + x^2b^4\right]^{1/2}}{b^2}$$

Equation (14) $$r_1 = \left(\frac{b^2}{a^4}\right){r_2}^3$$

Equation (17) $$\sigma_1 = \frac{pr_2}{2h}$$

Equation (18) $$\sigma_2 = \frac{pr_2}{2h}\left(2 - \frac{r_2}{r_1}\right).$$

Note that these equations are valid for computing overall average stresses through the thickness of the membrane regardless of the material properties.

Equation (18) shows that compressive hoop stresses will appear at equatorial locations in domes with $r_1 > 2r_2$. Of particular interest is the *a/b* ratio required to keep all hoop stresses greater than zero. Looking at an ellipse, one can visualize that r_1 increases dramatically and r_2 increases only slightly as one moves from the equator toward the apex. This means that the minimum hoop stress is at the equator as seen from equation (18). To find the *a/b* ratio for a zero hoop stress at the equator, equation (9) is substituted into equation (18) while setting $x = a$ and $y = 0$ (the location of the dome equator). This yields $a/b = \sqrt{2}$. Low-profile domes are those that have an *a/b* ratio $> \sqrt{2}$. By substituting appropriate values of *a* and *b* into equation (9) such that $a/b > \sqrt{2}$ and setting $x = a$ and $y = 0$, one can use equations (13) and (18) to show that the hoop stresses are negative (compressive) at the dome equator.

Equatorial buckling becomes a concern in low-profile domes that have high compressive hoop stresses.

High-strength composites have the capability, when appropriately oriented, to handle the high principal stresses encountered at the apexes of a low-profile dome as well as the high compressive stresses near the dome equator. It is therefore feasible to design a composite dome of varying thicknesses and layup angles to meet the different stress states at different meridional locations.

B. Application to Composites

To design a low-profile dome using composite materials, it is useful to look at the hoop and meridional line loads (which are equal to the corresponding stress multiplied by the thickness). This is very helpful in design since thicknesses are initially unknown and must be selected. Using the equations derived above, a table of hoop and meridional load versus coordinate location on the dome can be derived. This is shown in table 1 for the tested dome, which had an equatorial diameter of 40.2 in. and a 3-to-1 radius-to-height ratio.

After having mapped the line loads as a function of position on the dome, the various stress states and potential failure modes must be considered. Several potential failure modes are possible in a low-profile dome: biaxial tension, biaxial tension-compression (shear), and hoop compression buckling. Since the dome was constructed by hand layup of individual gore sections, the resulting seams weaken the design and must be compensated for to prevent premature failure. Test hardware and support equipment also influenced the dome's design; potential shearout at the bolted joint interface between the dome and the supporting base plate was a major concern.

Table 1. Loads of low-profile composite dome as a function of position, 100 psi internal pressure.

x_1 (in.)	x_2 (in.)	y_1 (in.)	y_1 (in.)	t (in.)	y_1 Mer. Load (lb/in.)	y_1 Hoop Load (lb/in.)	y_2 Mer. Load (lb/in.)	y_2 Hoop Load (lb/in.)
20.1	19.58979326	0.0	1.5	0.24	1005.00	–7035.00	1189.55	–5262.65
19.5897933	19.43914924	1.5	1.7039	0.225	1189.55	–5262.65	1237.99	–4866.76
19.4391492	19.27653878	1.7039	1.8981	0.21	1237.99	–4866.76	1287.84	–4482.84
19.2765388	19.10392627	1.8981	2.083	0.195	1287.84	–4482.84	1338.29	–4115.82
19.1039263	18.92284699	2.083	2.2592	0.18	1338.29	–4115.82	1388.79	–3767.84
18.922847	18.73479838	2.2592	2.4271	0.165	1388.79	–3767.84	1438.88	–3439.82
18.7347984	18.5410955	2.4271	2.5871	0.15	1438.88	–3439.82	1488.21	–3131.72
18.5410955	18.34274775	2.5871	2.7397	0.135	1488.21	–3131.72	1536.59	–2842.69
18.3427478	18.15228585	2.7397	2.8772	0.12	1536.59	–2842.69	1581.18	–2586.68
18.1522858	17.94942041	2.8772	3.0153	0.105	1581.18	–2586.68	1626.83	–2334.01
17.9494204	11.414	3.0153	5.5149	0.06	1626.83	–2334.01	2521.21	1436.90
11.414	11.172	5.5149	5.5697	0.075	2521.21	1436.90	2659.31	1900.34
11.272	10.927	5.5697	5.6235	0.09	2659.31	1900.34	2677.94	1961.38
10.927	6.734862166	5.6235	6.3127	0.105	2677.94	1961.38	2860.60	2543.48
6.73486217	6.48678655	6.3127	6.3415	0.12	2860.60	2543.48	2872.05	2579.03
6.48678655	6.237757789	6.3415	6.3692	0.135	2872.05	2579.03	2883.06	2613.14
6.23775779	5.989716668	6.3692	6.3956	0.15	2883.06	2613.14	2893.56	2645.58
5.98971667	5.740939706	6.3956	6.4209	0.165	2893.56	2645.58	2903.63	2676.61
5.74093971	5.492519913	6.4209	6.445	0.18	2903.63	2676.61	2913.22	2706.11
5.49251991	5.243546891	6.445	6.468	0.195	2913.22	2706.11	2922.38	2734.22
5.24354689	4.99407468	6.468	6.4899	0.21	2922.38	2734.22	2931.11	2760.93
4.99407468	4.745396586	6.4899	6.5106	0.225	2931.11	2760.93	2939.36	2786.14
4.74539659	4.496486588	6.5106	6.5302	0.24	2939.36	2786.14	2947.18	2809.97
4.49648659	4.246053113	6.5302	6.5488	0.255	2947.18	2809.97	2954.60	2832.56
4.24605311	3.996893549	6.5488	6.5662	0.27	2954.60	2832.56	2961.54	2853.66
3.99689355	3.747831873	6.5662	6.5825	0.285	2961.54	2853.66	2968.05	2873.40

NOTE: x_1, x_2 are radial coordinates; y_1, y_2 are axial coordinates

NOTE: Ply angles are measured with respect to circumferential direction (e.g., 0° is circumferential direction)

C. Design Derivation

The dome was designed using composite laminate theory to meet a 100 psi internal pressure limit load. The line loads were input into the equations for a laminate to derive the stresses and strains of the laminate by using a weighted average of all the lamina stiffnesses in a given direction in the laminate. The total strain through the thickness was assumed constant. In addition, the laminate was assumed to be stacked in a manner symmetric about its centerline. This was not the case in the actual hardware, although the majority of the plies were of 0° and 90° orientations, whose stiffness and strength properties were similar to each other. At 100 psi pressure, the ply layups were chosen to give a safety factor of at least 2.0 on first ply failure (FPF) based on the biaxial tension or biaxial tension-compression with the Tsai-Hill failure criterion. This was the case because other failure modes (failure at seams, buckling) were thought to occur well before twice the limit load. The goal was to ensure that the dome would meet an ultimate safety factor of 1.4 against these other modes.

To determine the actual ply layups, a FORTRAN computer code was written to calculate lamina stresses and strains based on the stated assumptions of constant strain through the shell thickness. A spreadsheet calculating the loads and overall stresses in the hoop and meridional directions as a function of dome position was prepared using the analytical equations described earlier in this report. These line loads were used as inputs into the FORTRAN program to generate the required layup to meet the safety factor of 2.0 on FPF. This was accomplished via a "cut and try" method of selecting a layup combination, running the FORTRAN program to determine if it met the safety factor, and then modifying the layup as necessary until a suitable combination was found. This procedure was repeated at various locations along the dome meridian from equator to apex such that a structurally acceptable layup profile was developed. The layup as a function of dome coordinate position is shown in table 1.

After a basic layup profile was found, design details could then be examined. One of these was the interface of the dome to the associated test fixture hardware, an arrangement which consisted of 75 9/16-in. diameter bolts. The resulting joint subjects the bolts to shear loads and the composite material around the bolt holes to bearing, tearout, and shearout loads. This joint was designed using a computer program known as the Bolted Joint Stress Field Model (BJSFM).[2] This software allows a designer to input ply orientations, thicknesses, loads, etc. and calculate the failure load of the joint. Using this tool, a layup arrangement using 0°, 90°, 45°, and -45° plies was devised. This ensured that this joint would fail at 339 psi, far above the expected dome failure loads in the 150- to 200-psi range.

As is explained in the next section, the dome was manufactured by hand from layers of precut gores in order to give the dome the correct shape when laid up on the mandrel. Such methods introduce seams in the finished product that run along the meridional direction from apex to equator. The resulting stress concentrations and shear concentrations were taken into account via a simple finite element analysis, which predicted failure stresses would be reached in the 150-psi range of internal pressure.

Additional analyses and design exercises were required to ensure no leaks would result during the test, to determine bolt torquing requirements, and to ensure structural integrity of the aluminum base plate and cover plate structures that were used in the test.

D. Manufacturing

The low-profile composite dome was manufactured using precut gore sections of IM7/8552 cloth graphite-epoxy material laid up by hand on a steel mandrel. This method, while labor-intensive, ensured that the dome would have adequate strength in both the hoop and meridional directions and allowed the number of layers and the resulting dome thickness to be easily varied as a function of stress state along the dome meridian. In effect, it allowed the dome to be design optimized; this would have been very difficult, to impossible, to accomplish using the state-of-the-art filament-winding or fiber-placement techniques of the time with their unidirectional tape arrangements. Tailoring the thicknesses of unidirectional tape to meet the stress state and even winding it in such a way as to resist the highly varying stress states encountered in a low-profile dome was, at the time, a very formidable task and would have resulted in a much heavier and thicker dome than resulted from the hand layup with the IM7/8552 cloth material and its highly bidirectional stiffness and strength properties.

The following procedure was used to manufacture the dome:

1. Gores (each sweeping 22.5°) were precut with proper orientations (0°, 90°,45°, and -45°) to the required lengths and widths for layup on the mandrel.

2. Sixteen full-length gores were laid on the mandrel to form the first layer of the dome, followed by subsequent layers offset 1 to 2 in., circumferentially. This was done to prevent continuous seams through the entire thickness or a large part of the thickness. Subsequent shorter gores were used to make the buildup areas near the equator and apex regions of the dome.

3. Debulking was performed periodically during the layup process to ensure that gores remained positionally stable and remove air bubbles. A vacuum bag was attached to the entire layup and evacuated, allowing atmospheric pressure to compress the layup against the mandrel.

4. After all gores were laid and a final debulk was performed, the dome was vacuum-bagged and autoclaved for more than 8 hr at 300 °F and a pressure higher than atmospheric.

5. A 4-in. diameter hole was drilled into the apex of the dome to accommodate the cover plate (which held the overflow and relief valves used in the test). Sixteen bolt holes for securing the cover plate were drilled around this large hole. The bottom of the dome below the equator was final-machined to bring the total dome height to 10.015 in. Seventy-five bolt holes for securing the equator to the base plate interface ring were also drilled.

The finished dome is shown in figure 3. The final dimensions of the dome were 40.2 in. in diameter and 10.015 in. in height (in final-machined configuration). The weight of the dome without the interface ring and the cover plate was approximately 11 lb. The interface ring used to bolt the dome to the base plate is shown in figure 4.

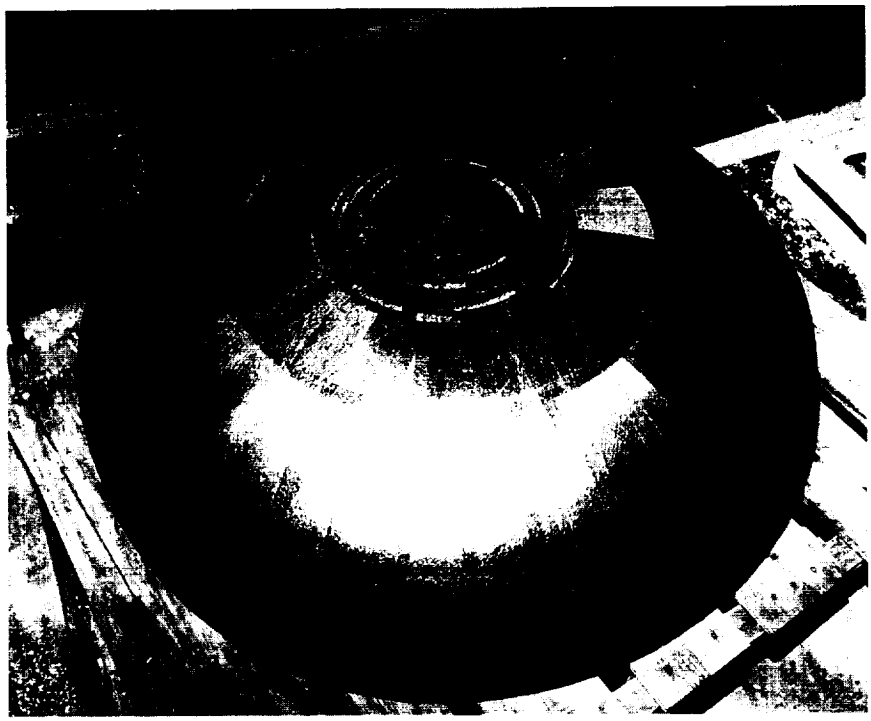

Figure 3. Completed low-profile composite dome.

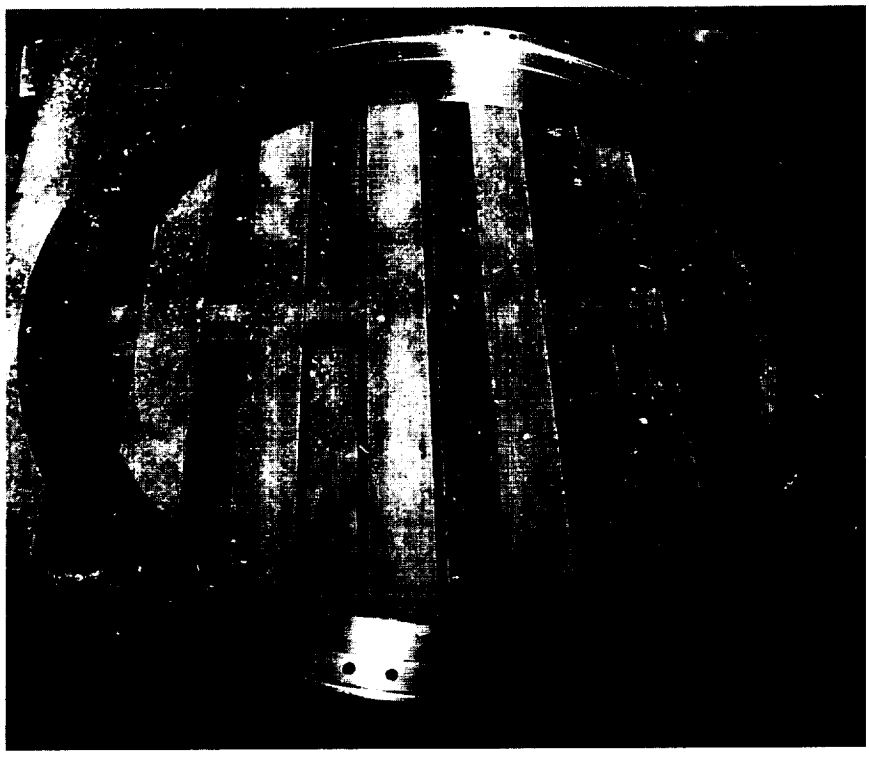

Figure 4. Interface ring used to secure dome to base plate.

III. ANALYSIS

Both analytical analysis and finite element methods were used to calculate predicted stresses, strains, displacements, and failure loads. Failure can occur in one or all of the following ways: circumferential hoop buckling, biaxial tension, and biaxial tension-compression (shear). As shown earlier, the stress state as a function of position on the dome was known analytically via the dome stress equations. Beginning with the known stress state, composite laminate theory was used to calculate the resulting strains and stresses in the material directions of the individual layers. These were then used to estimate the expected failure loads via the Tsai-Hill failure criterion.

A. Analytical Solutions

Since the overall stress state was known, finite element analysis was not necessary to determine the stresses and strains at a given point in the dome. These were determined using established methods of composite laminate theory treated by Tsai and Hahn[3] and other authors. The detailed methods are described in their books and only an outline of the procedure is given here. It should be noted at this point that only in-plane stiffness analysis was used here, which meant that any asymmetry in the layups was ignored. This was done because the stiffness and strength properties of the IM7/8552 cloth material were similar in their orthogonal directions and, therefore, asymmetry was not considered to affect the resulting solutions. Time and manpower constraints prevented the more detailed approach of evaluating the in-plane/bending moment coupled stiffnesses and the bending stiffnesses. The same FORTRAN program used to derive the layup was also used to determine the on-axis ply stresses and strains given the stress state known via the dome stress equations in the circumferential-meridional dome coordinate system.

The material properties of the IM7/8552 cloth material are shown in table 2. The warp and fill stiffnesses were both approximately 12 msi and their strengths approximately 125 to 130 ksi in the orthogonal directions. The test strain and displacement predictions are shown with their corresponding actual gauge readings in figures 5 through 52.

Table 2. Material properties of IM7/8552 graphite composite cloth material.

Material Properties For IM7/8552 Material				
Material Direction	**Tensile Strength (ksi)**	**Comp. Strength (ksi)**	**Tensile Modulus (Msi)**	**Comp. Modulus (Msi)**
Warp	133	94	12.1999999	10.5
Fill	128	94	11.8	10.5
Material Direction	**Shear Strength (ksi)**	**Shear Modulus (Msi)**	**Poisson's Ratio**	
Warp-Fill	12.3999999	0.63999999	0.3	

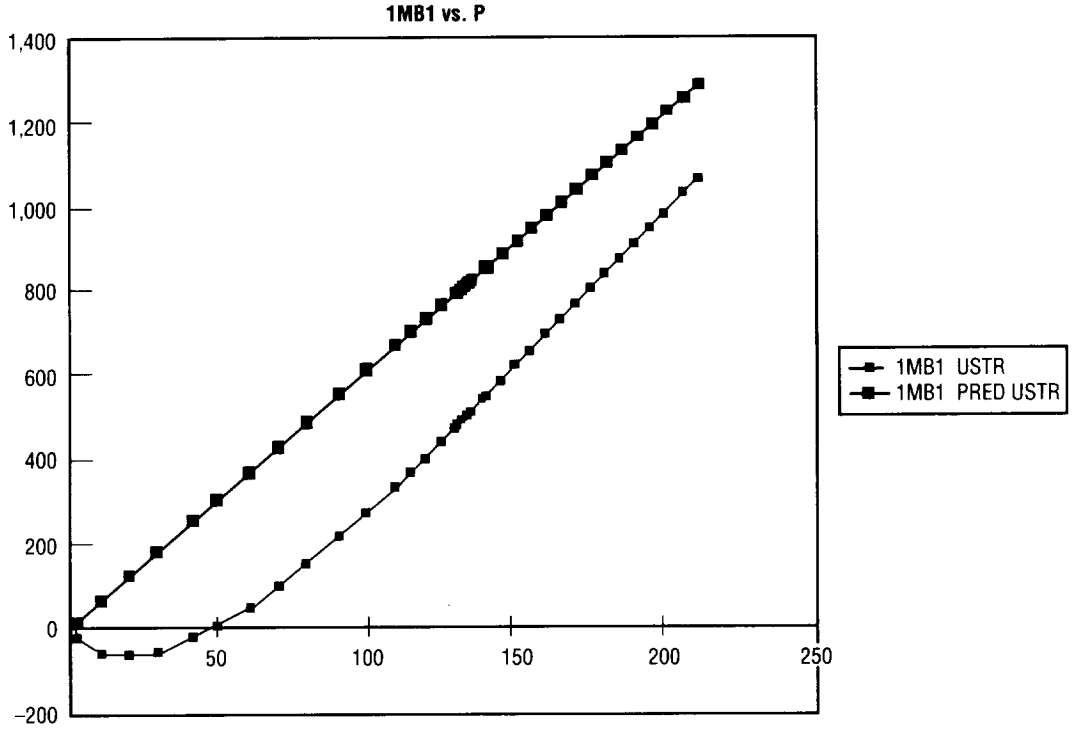

Figure 5. Predicted and actual meridional strains versus pressure, gauge 1MB1.

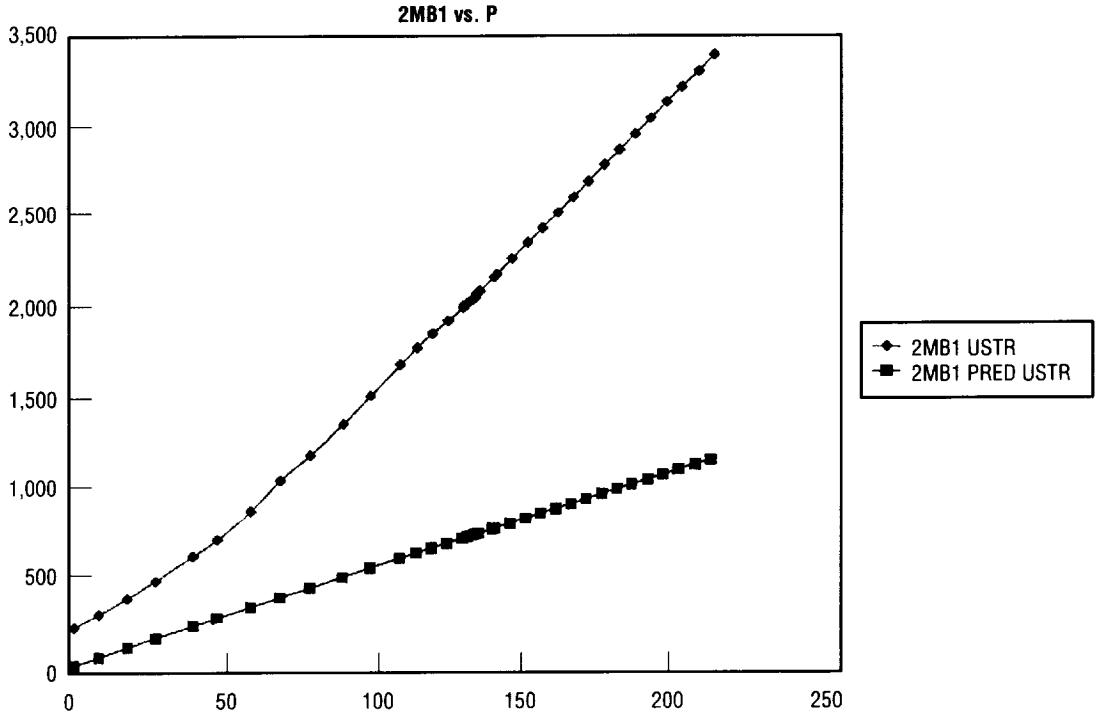

Figure 6. Predicted and actual circumferential strains versus pressure, gauge 2MB1.

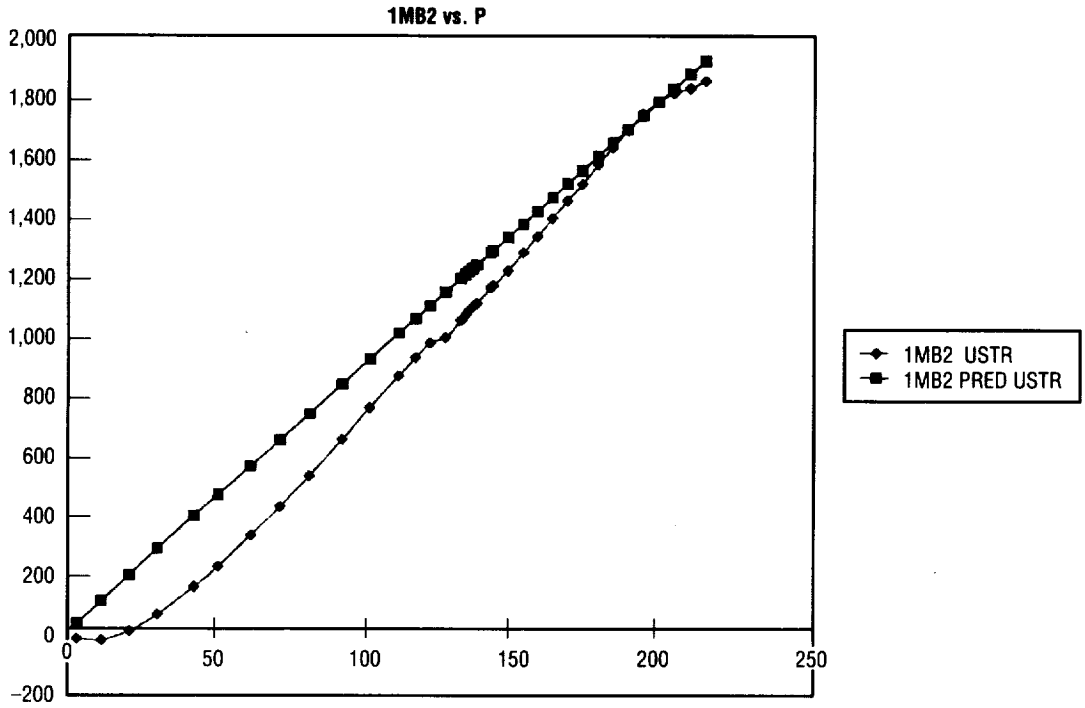

Figure 7. Predicted and actual meridional strains versus pressure, gauge 1MB2.

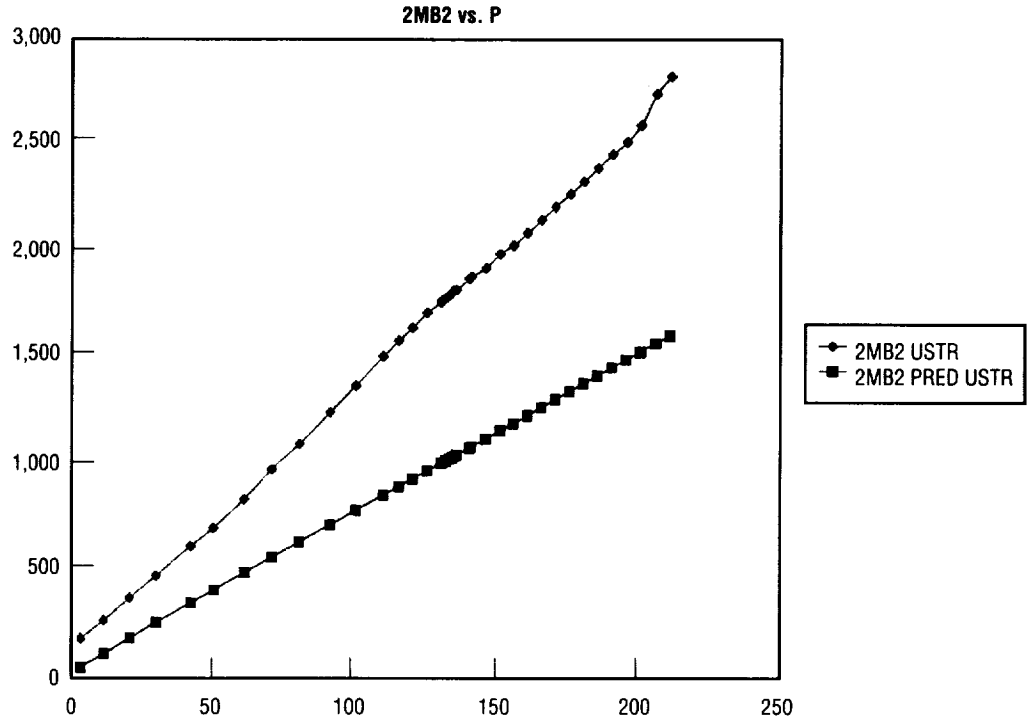

Figure 8. Predicted and actual circumferential strains versus pressure, gauge 2MB2.

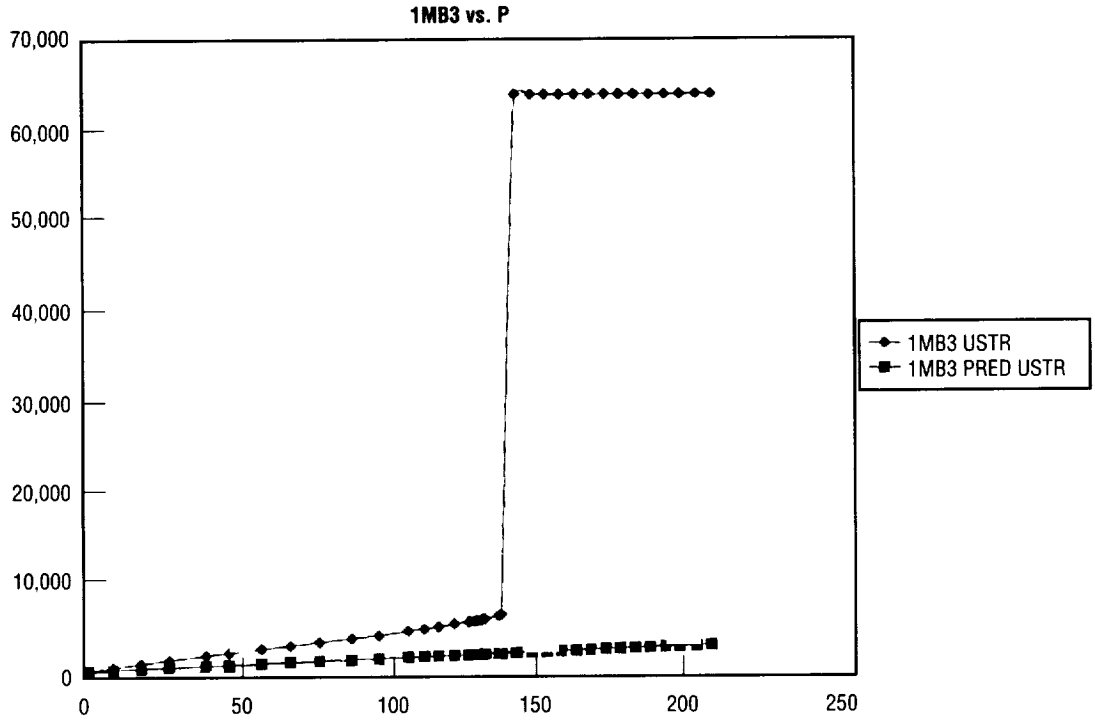

Figure 9. Predicted and actual meridional strains versus pressure, gauge 1MB3.

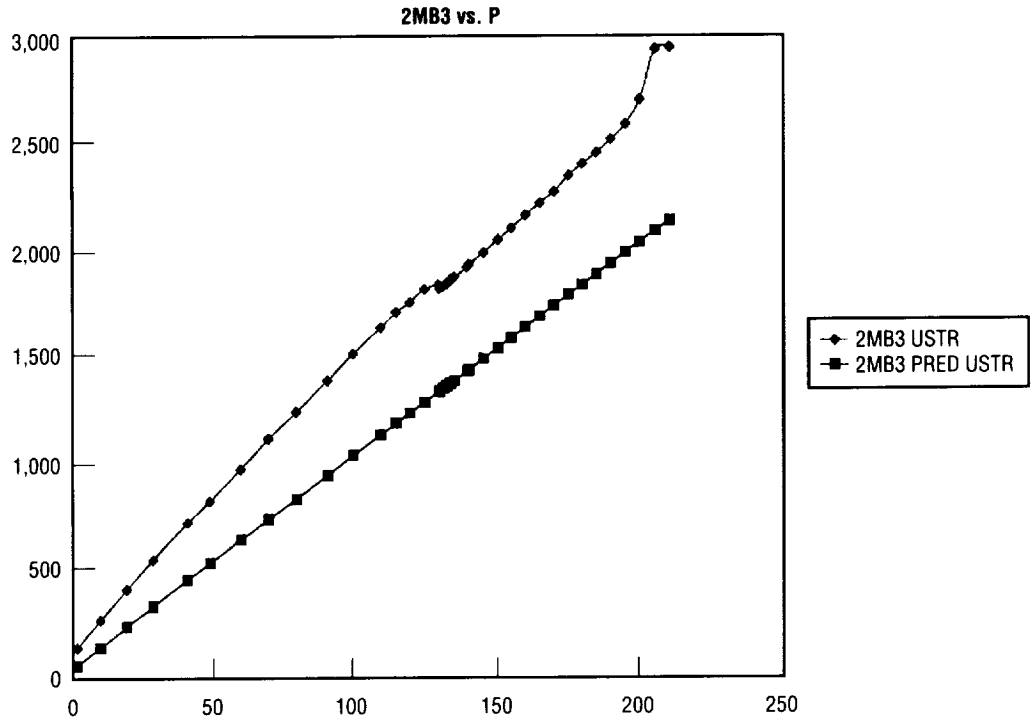

Figure 10. Predicted and actual circumferential strains versus pressure, gauge 2MB3.

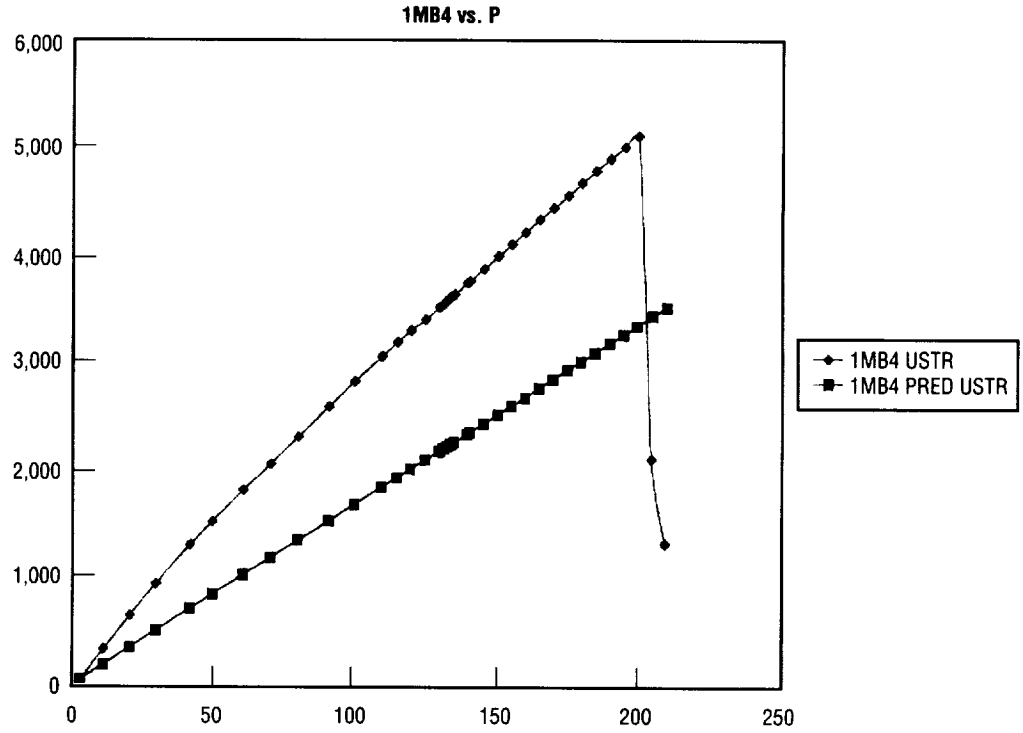

Figure 11. Predicted and actual meridional strains versus pressure, gauge 1MB4.

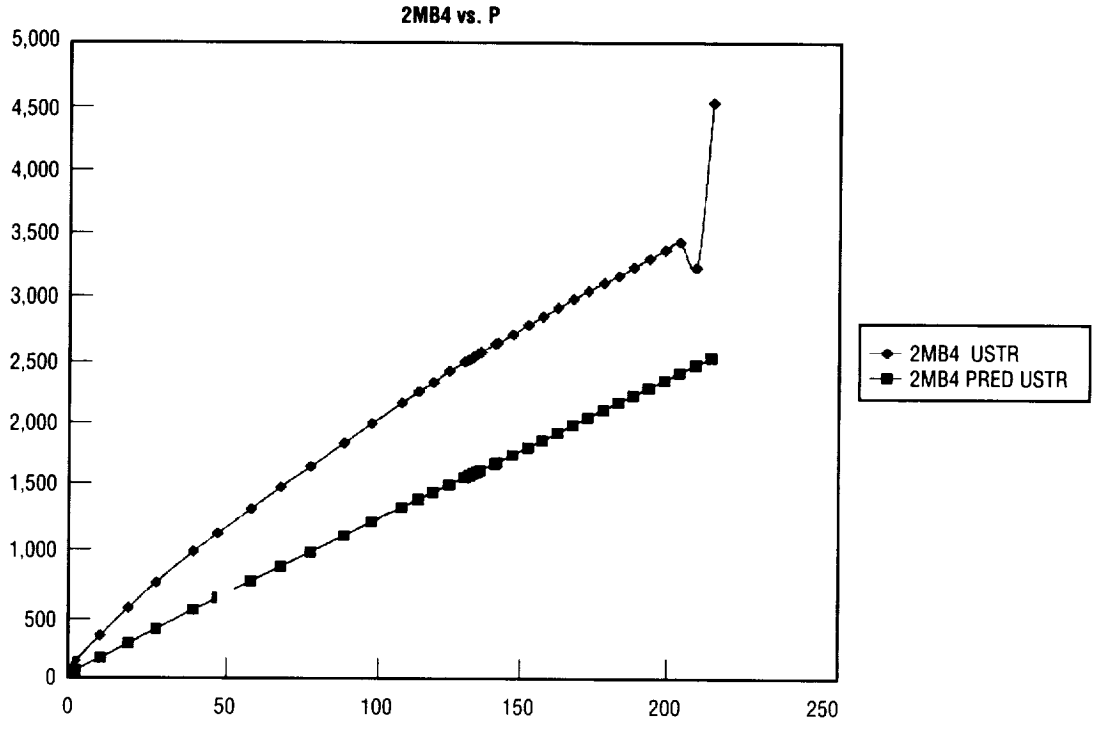

Figure 12. Predicted and actual circumferential strains versus pressure, gauge 2MB4.

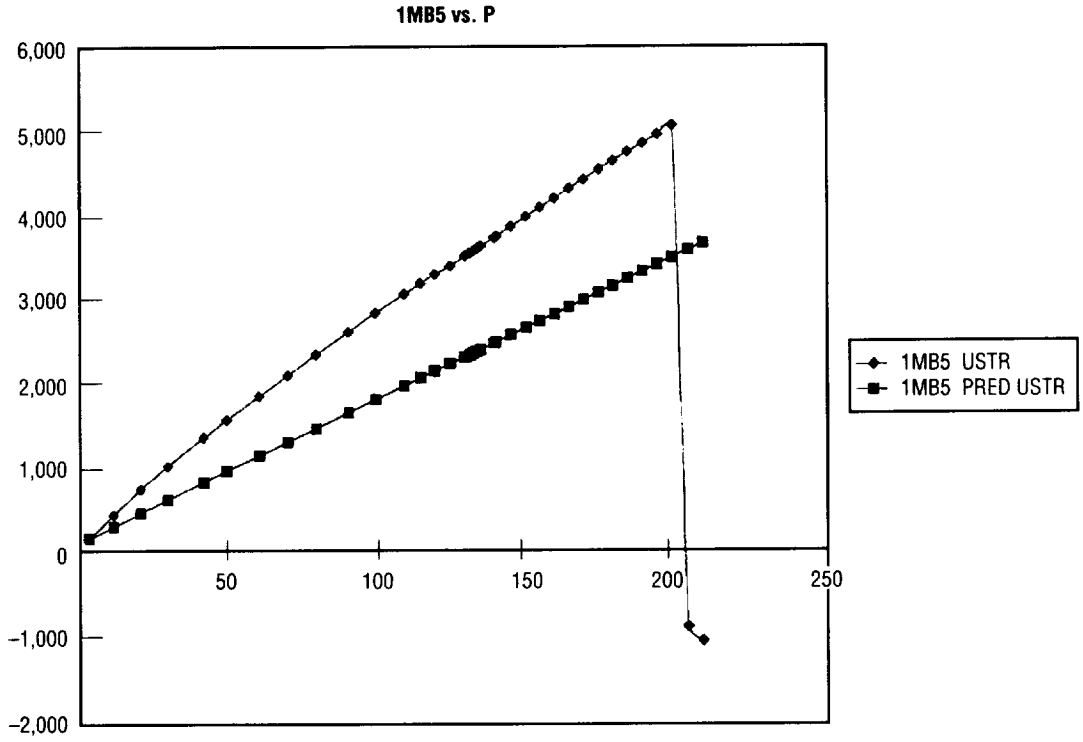

Figure 13. Predicted and actual meridional strains versus pressure, gauge 1MB5.

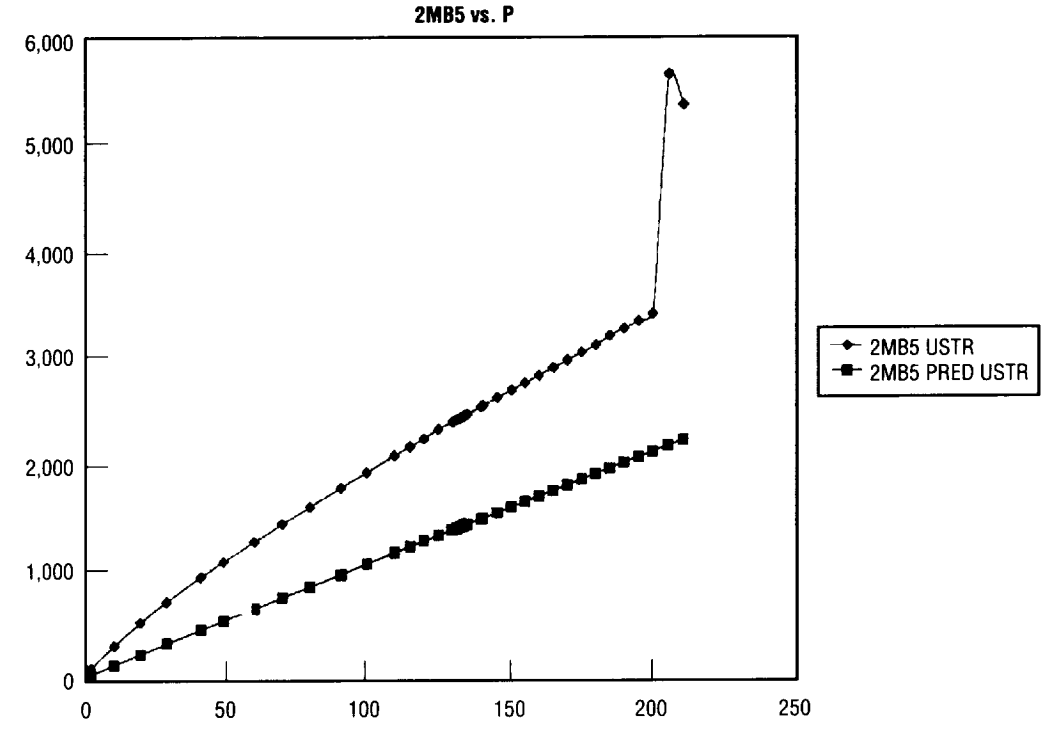

Figure 14. Predicted and actual circumferential strains versus pressure, gauge 2MB5.

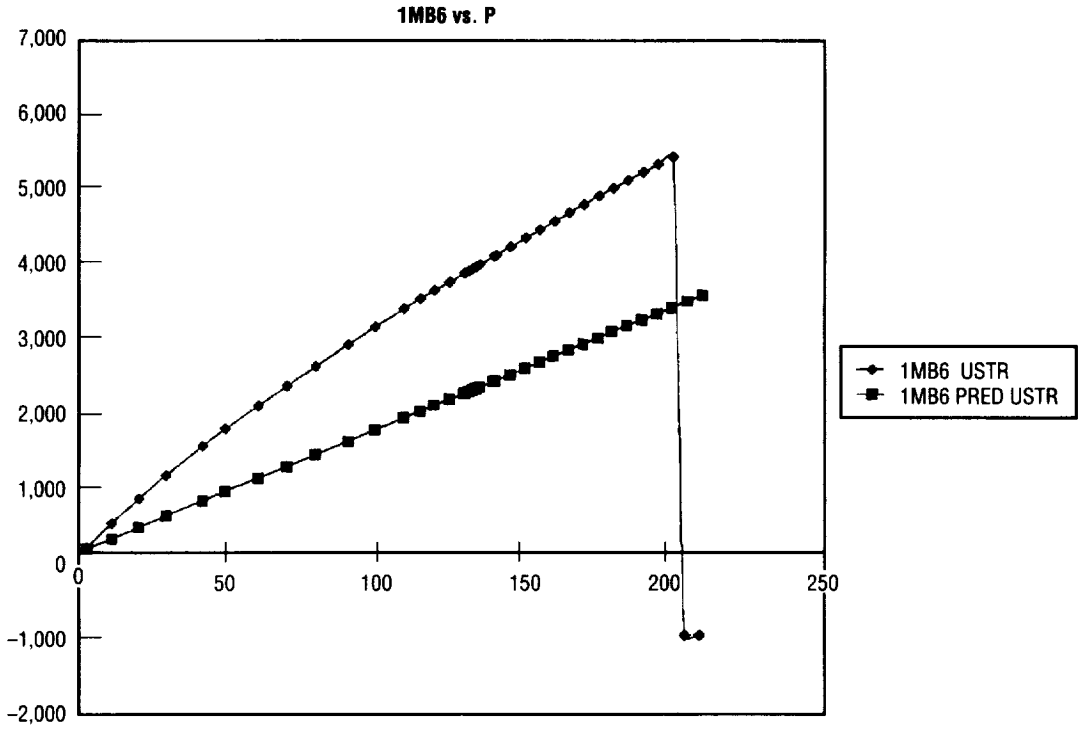

Figure 15. Predicted and actual meridional strains versus pressure, gauge 1MB6.

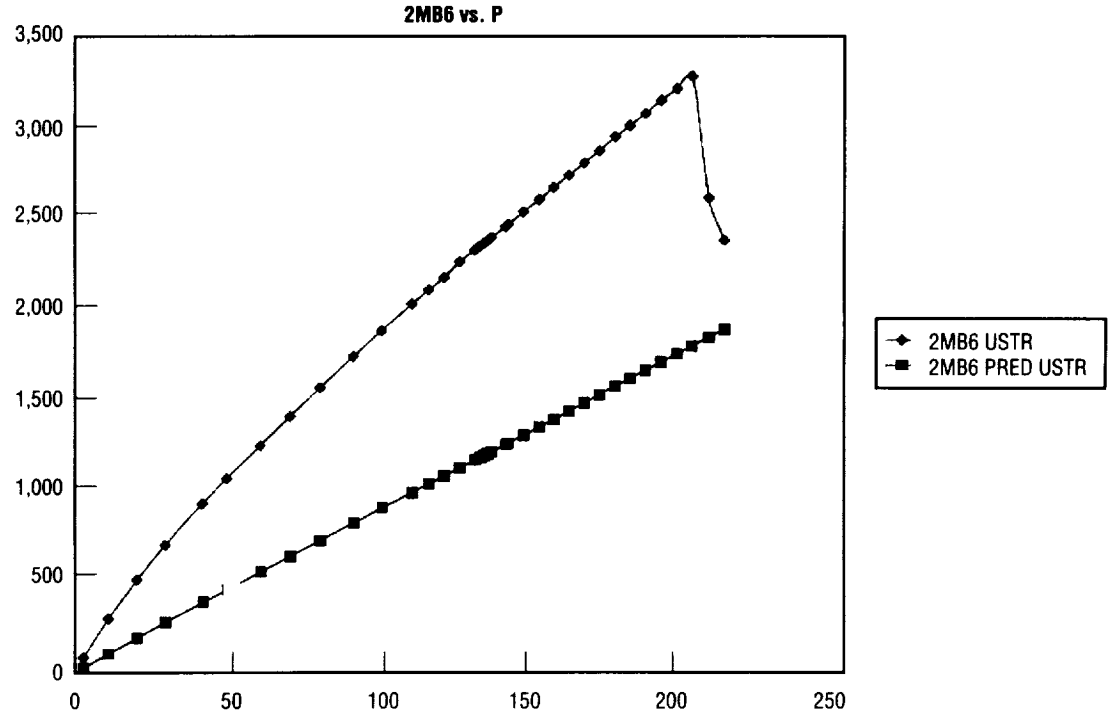

Figure 16. Predicted and actual circumferential strains versus pressure, gauge 2MB6.

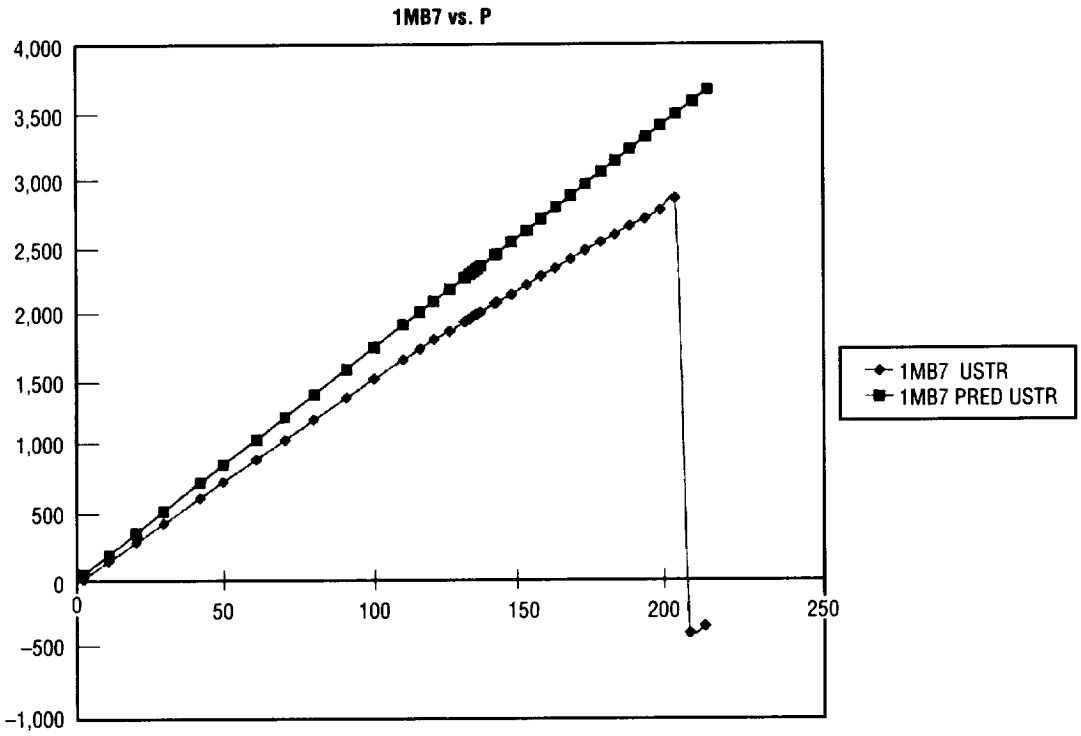

Figure 17. Predicted and actual meridional strains versus pressure, gauge 1MB7.

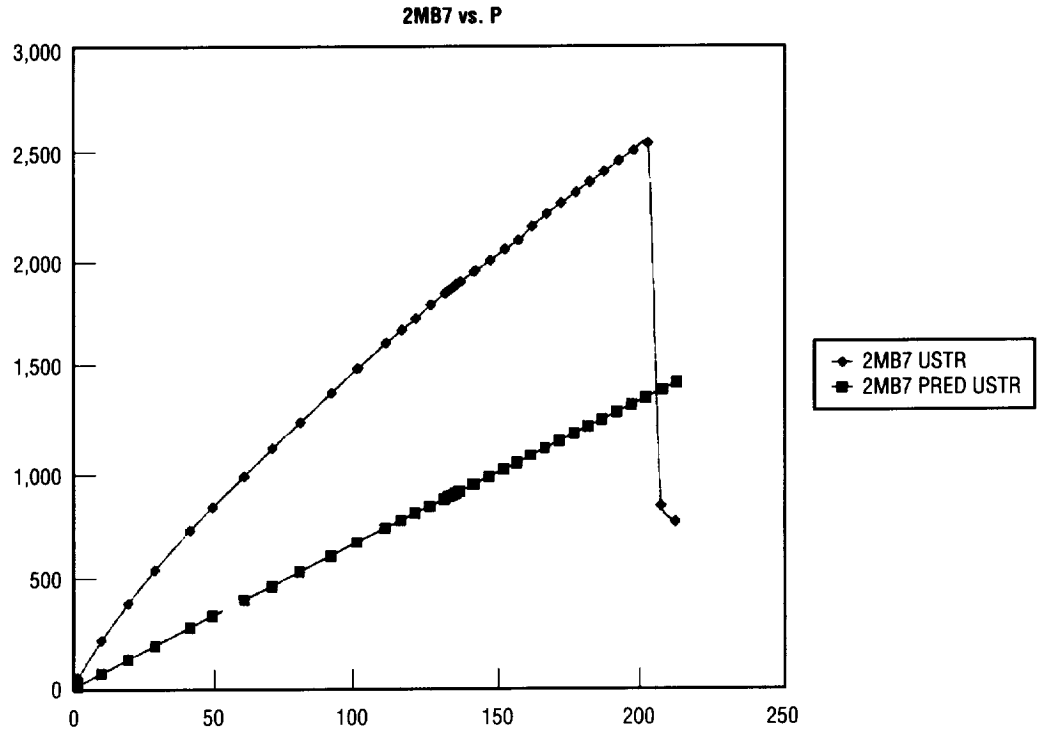

Figure 18. Predicted and actual circumferential strains versus pressure, gauge 2MB7.

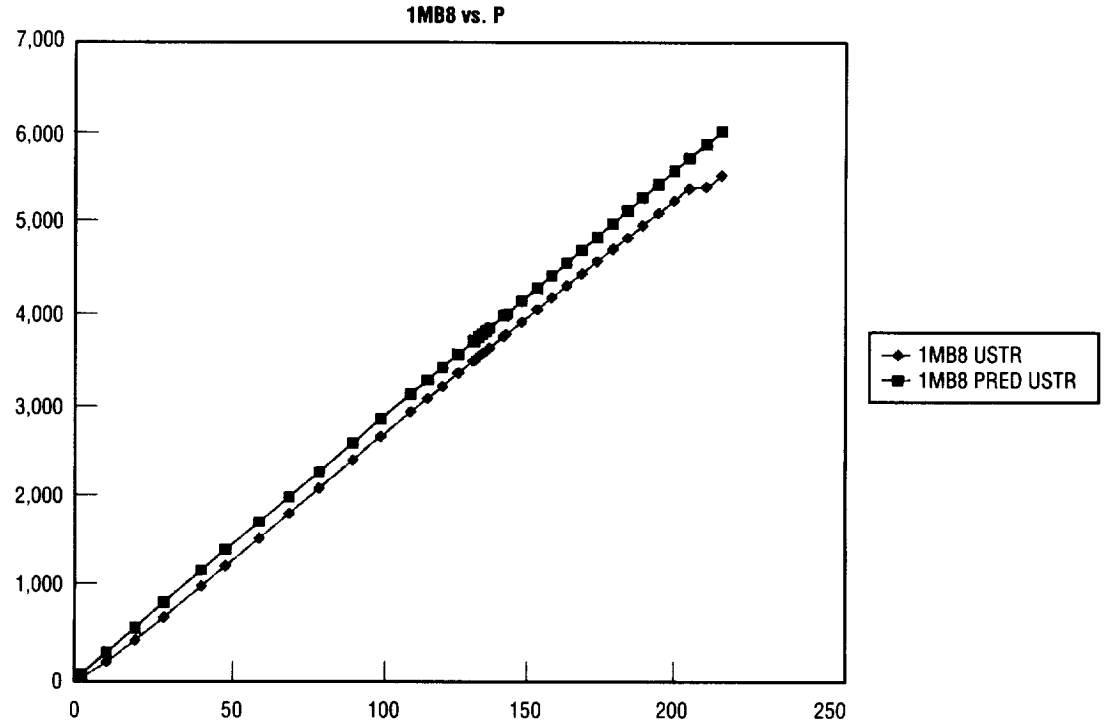

Figure 19. Predicted and actual meridional strains versus pressure, gauge 1MB8.

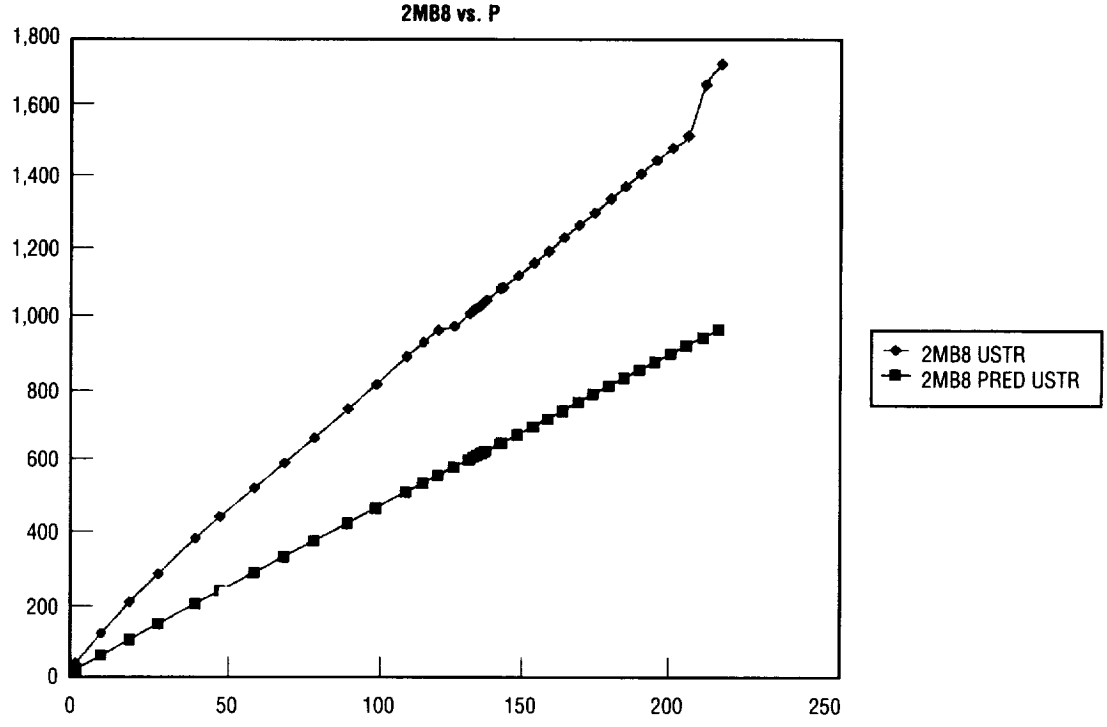

Figure 20. Predicted and actual circumferential strains versus pressure, gauge 2MB8.

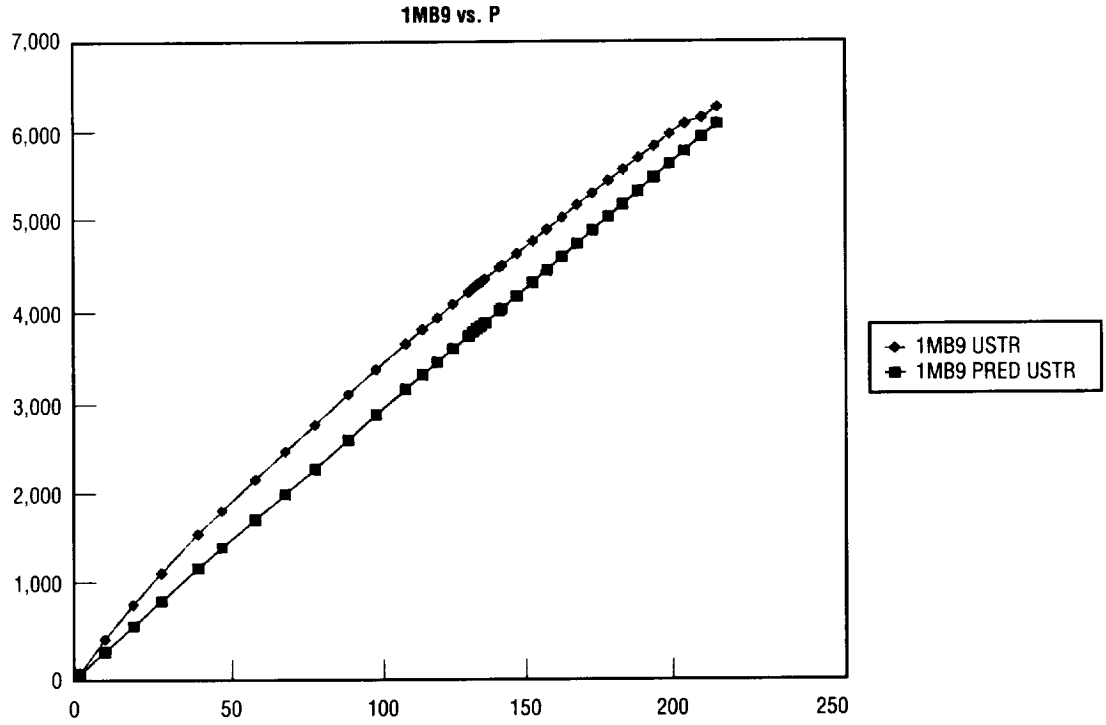

Figure 21. Predicted and actual meridional strains versus pressure, gauge 1MB9.

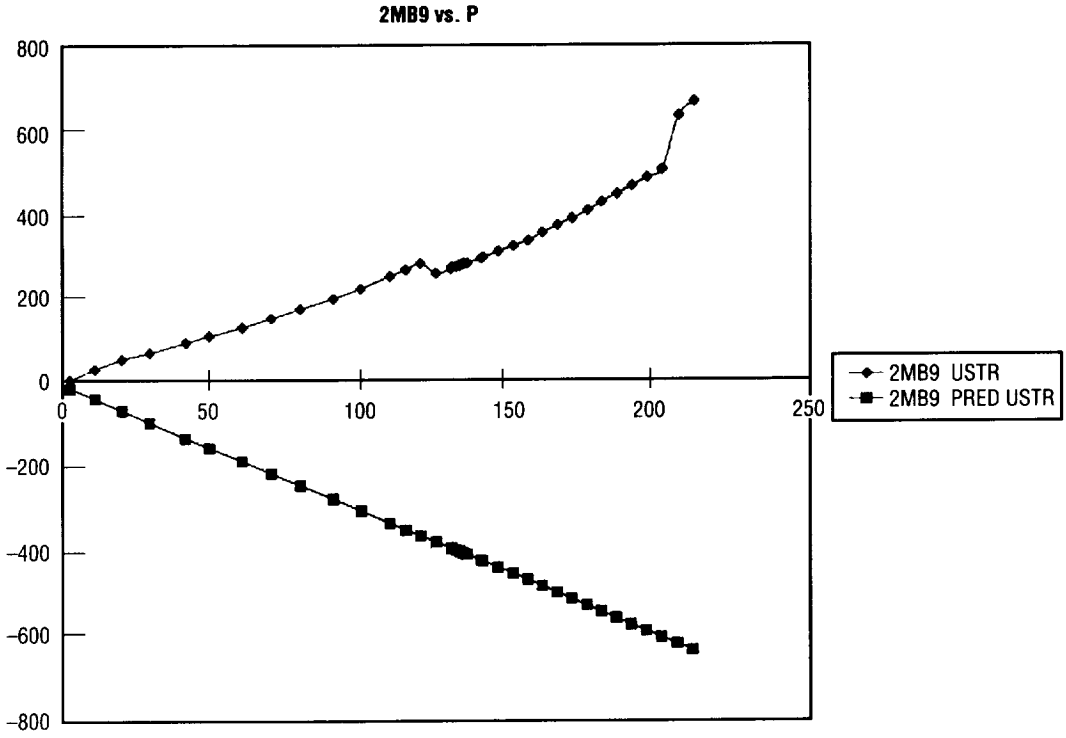

Figure 22. Predicted and actual circumferential strains versus pressure, gauge 2MB9.

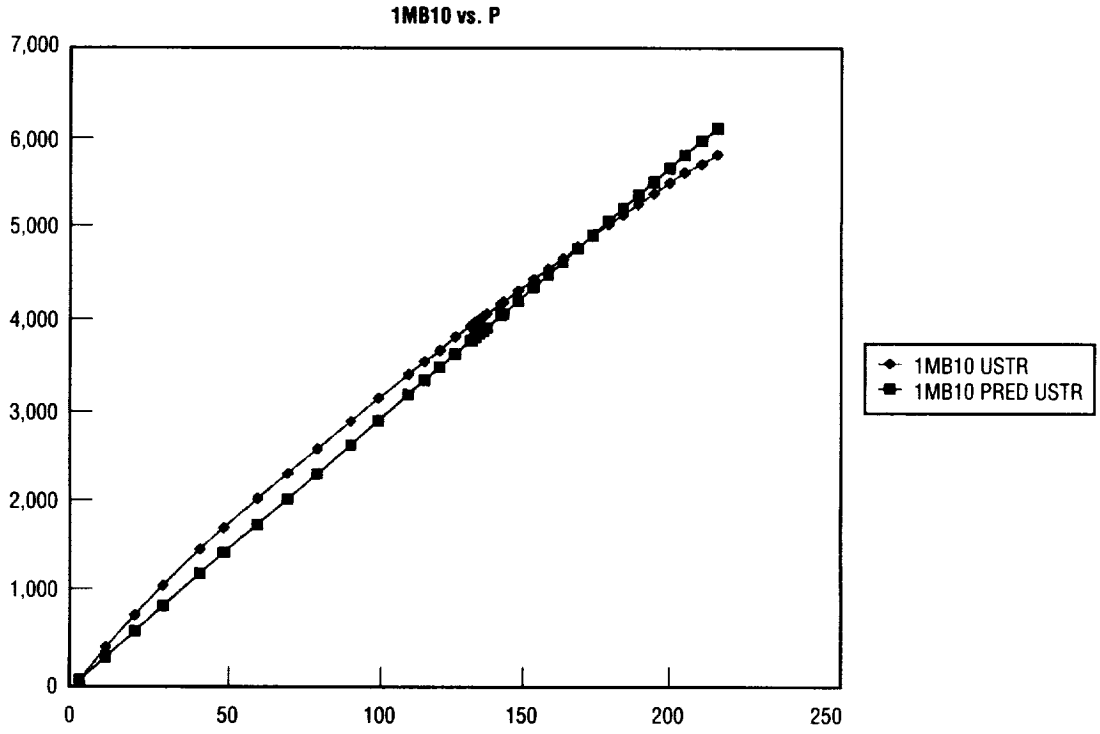

Figure 23. Predicted and actual meridional strains versus pressure, gauge 1MB10.

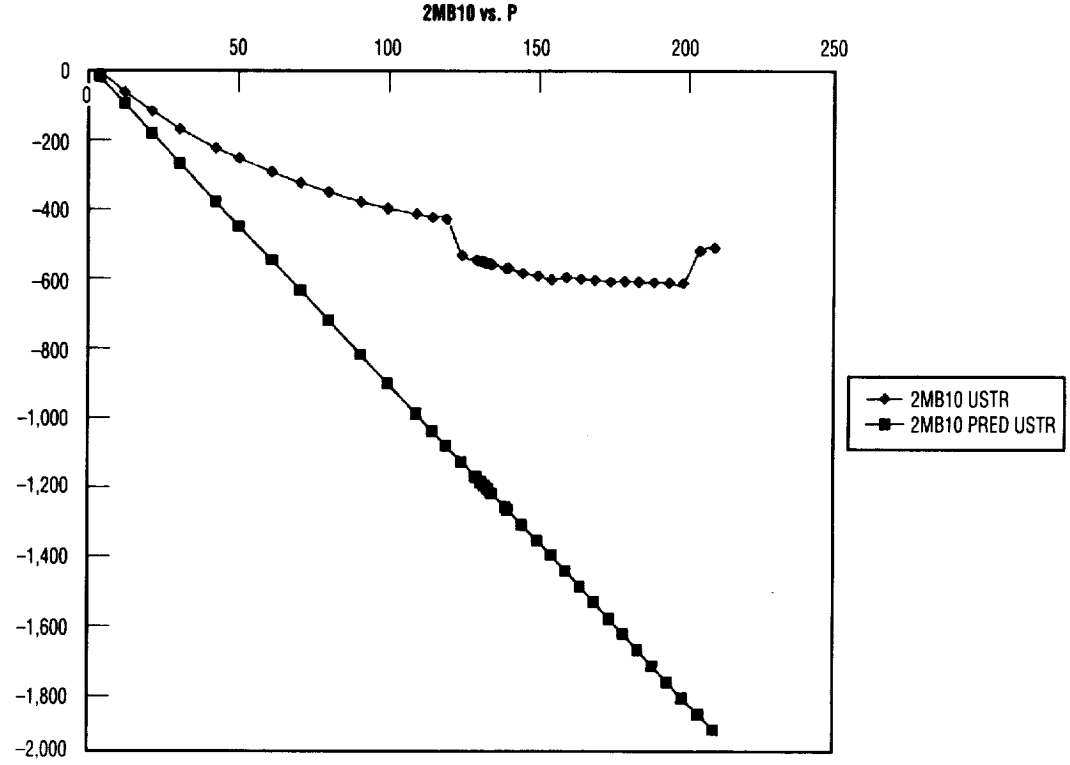

Figure 24. Predicted and actual circumferential strains versus pressure, gauge 2MB10.

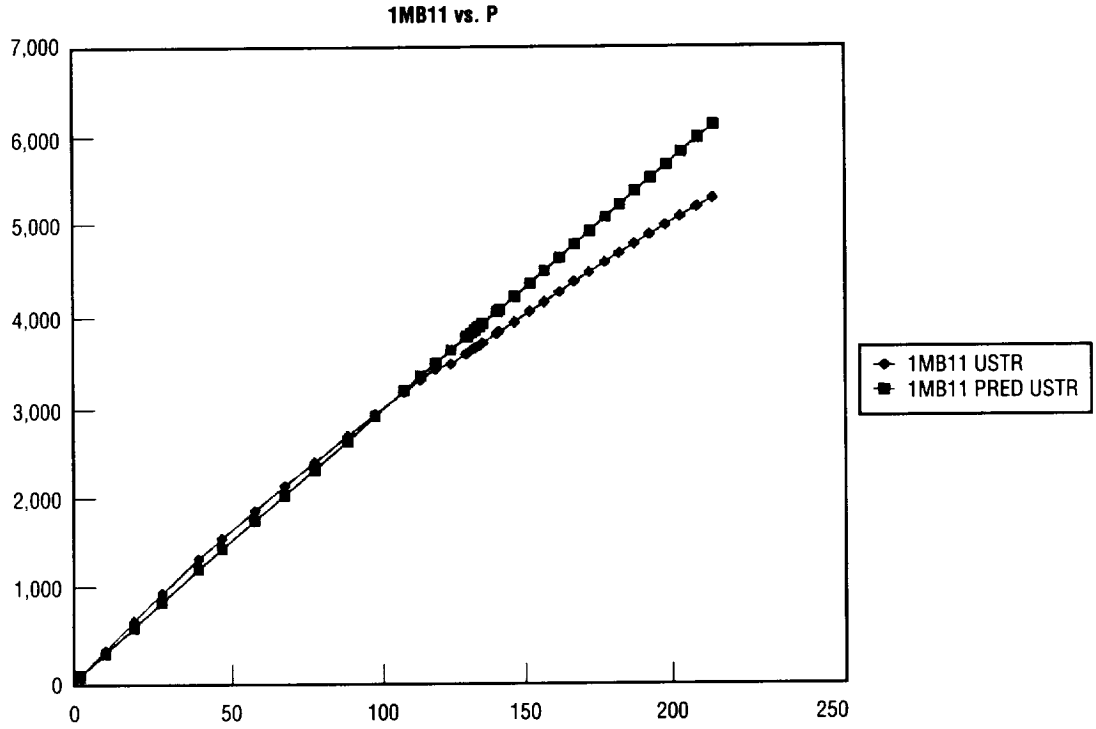

Figure 25. Predicted and actual meridional strains versus pressure, gauge 1MB11.

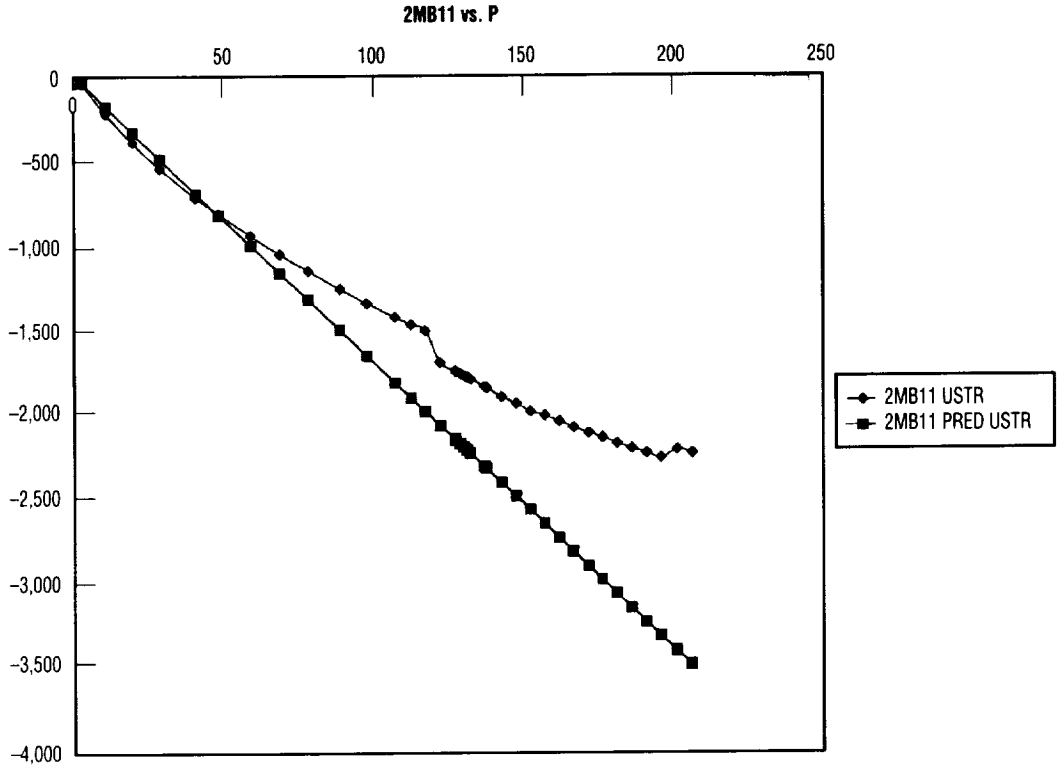

Figure 26. Predicted and actual circumferential strains versus pressure, gauge 2MB11.

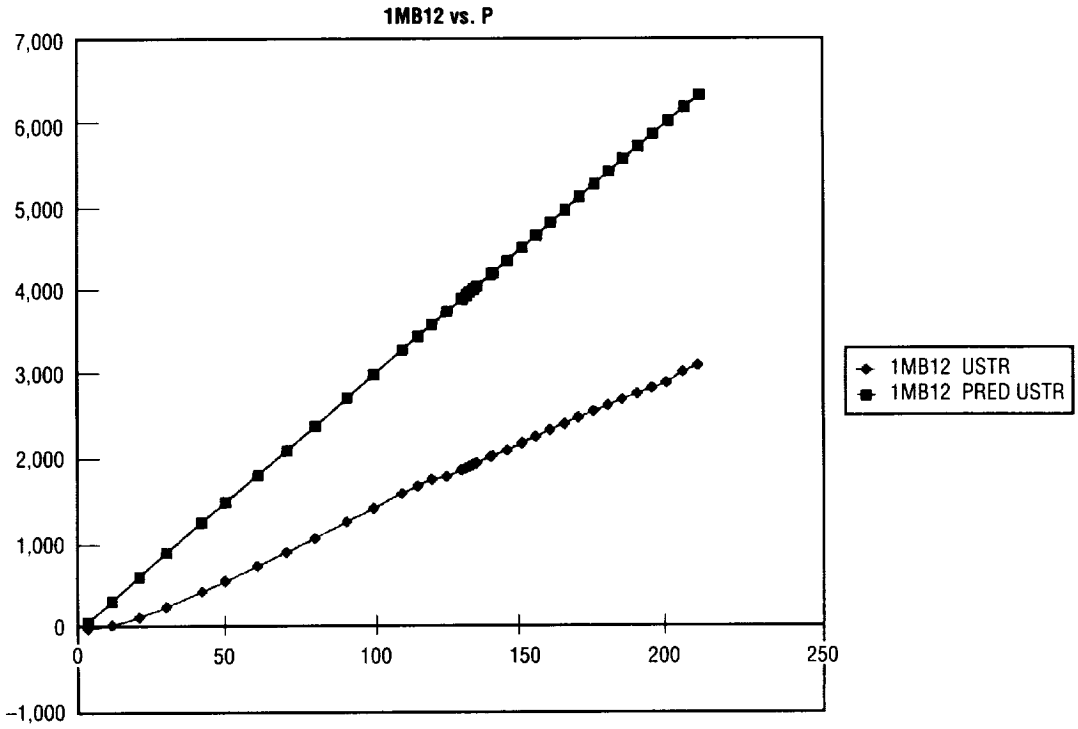

Figure 27. Predicted and actual meridional strains versus pressure, gauge 1MB12.

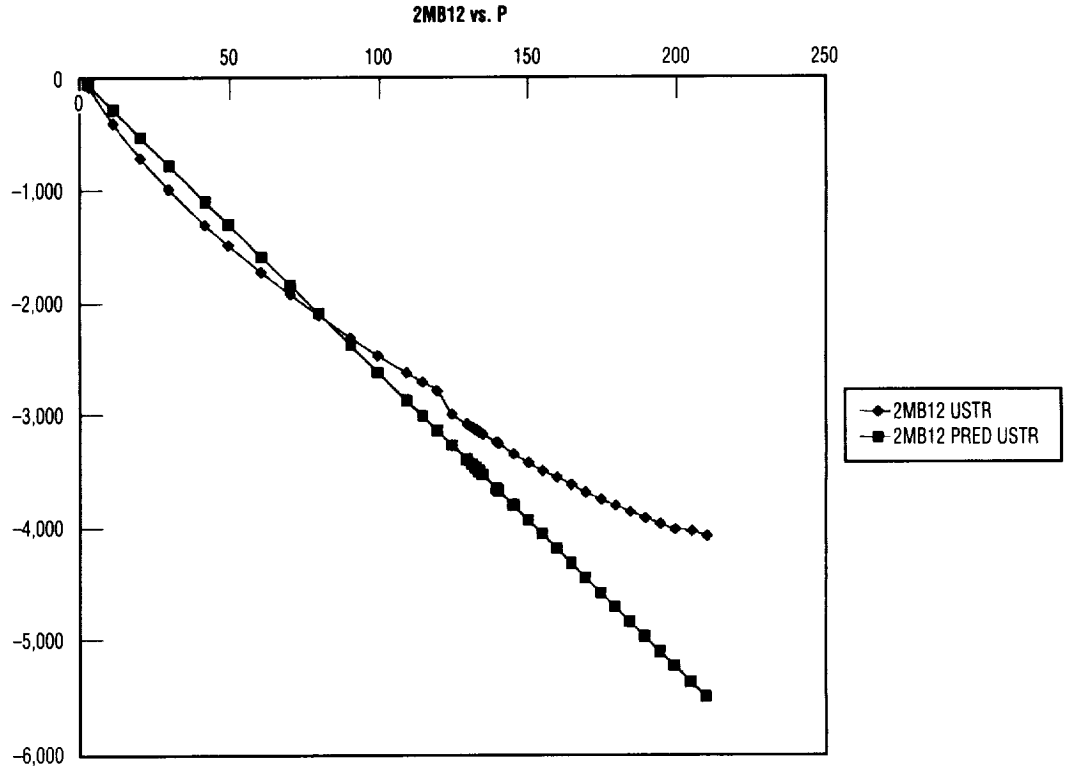

Figure 28. Predicted and actual circumferential strains versus pressure, gauge 2MB12.

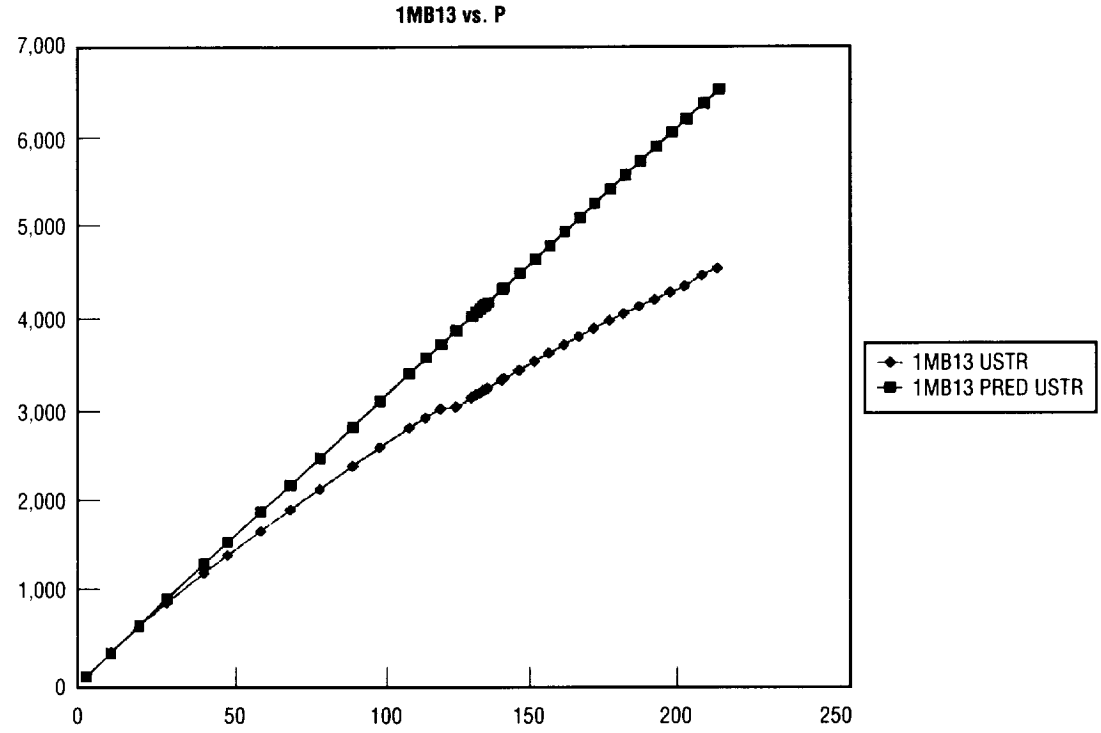

Figure 29. Predicted and actual meridional strains versus pressure, gauge 1MB13.

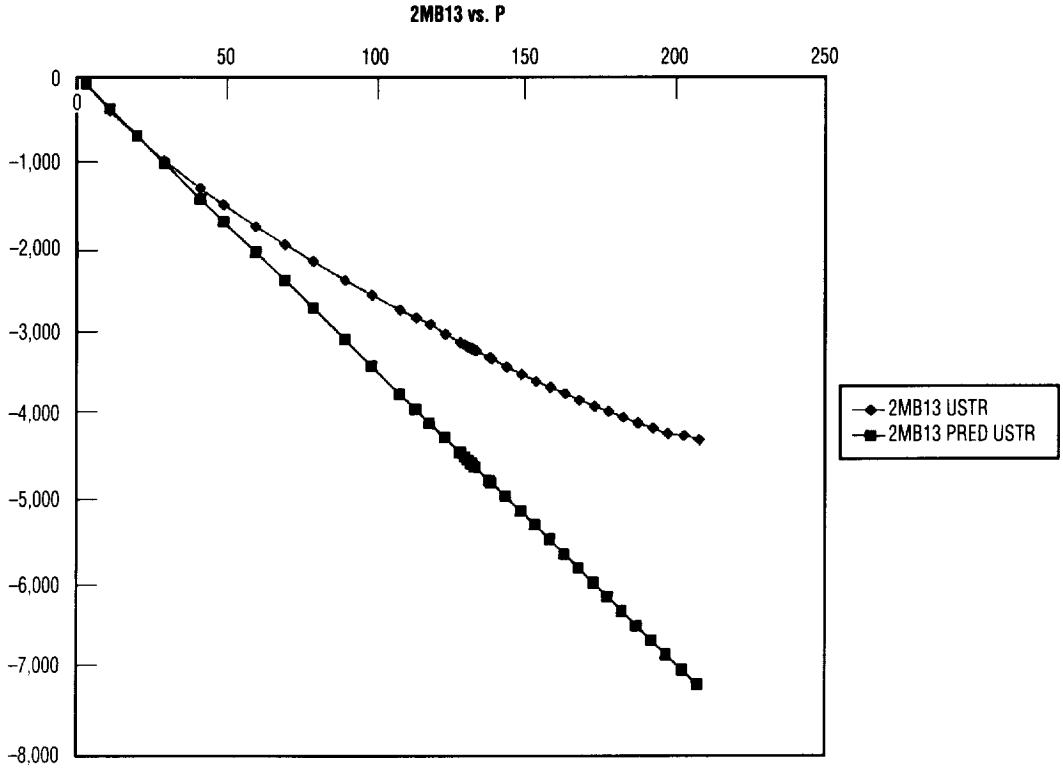

Figure 30. Predicted and actual circumferential strains versus pressure, gauge 2MB13.

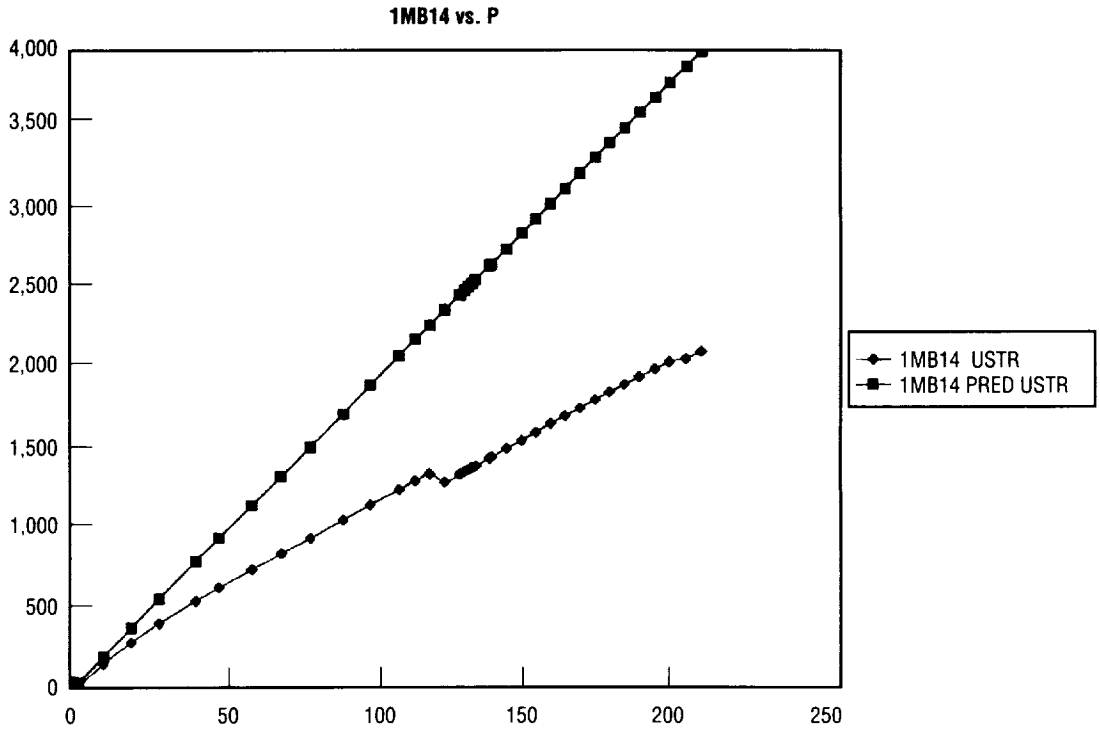

Figure 31. Predicted and actual meridional strains versus pressure, gauge 1MB14.

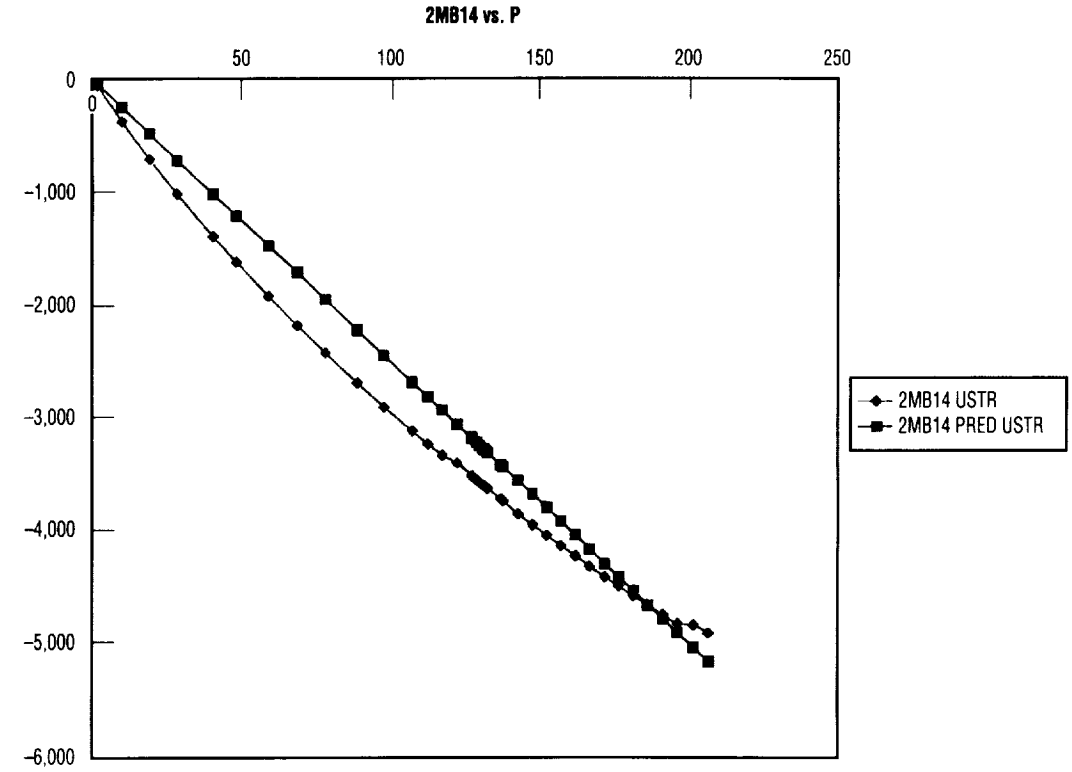

Figure 32. Predicted and actual circumferential strains versus pressure, gauge 2MB14.

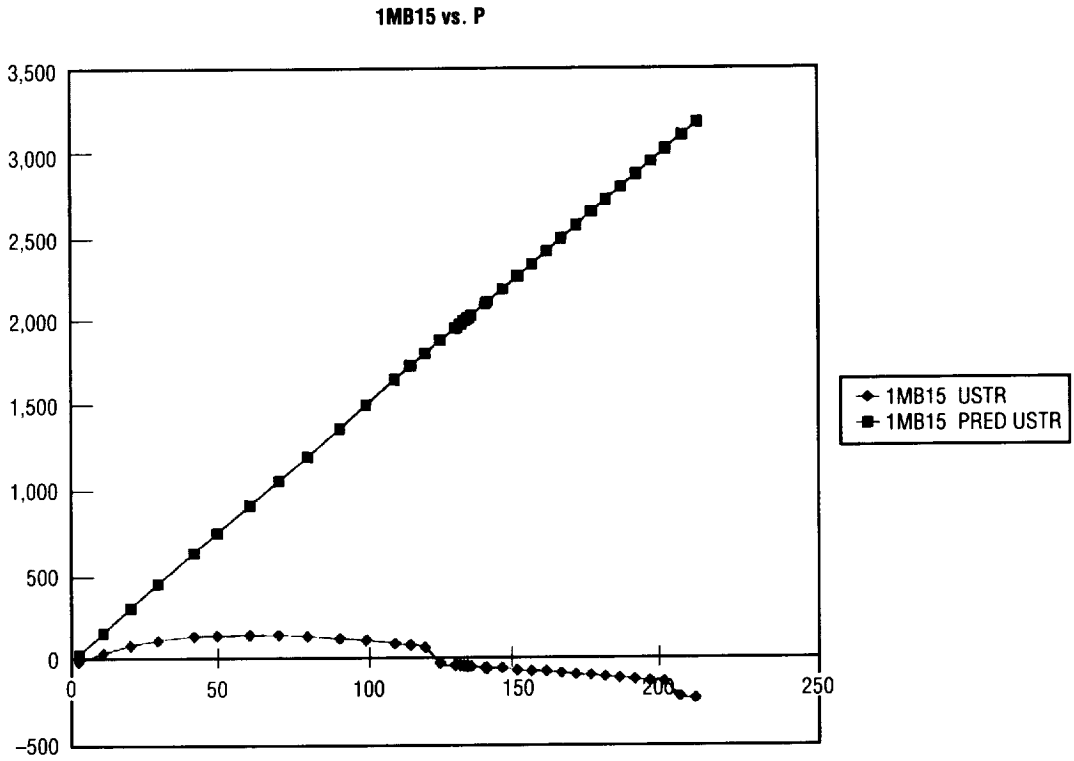

Figure 33. Predicted and actual meridional strains versus pressure, gauge 1MB15.

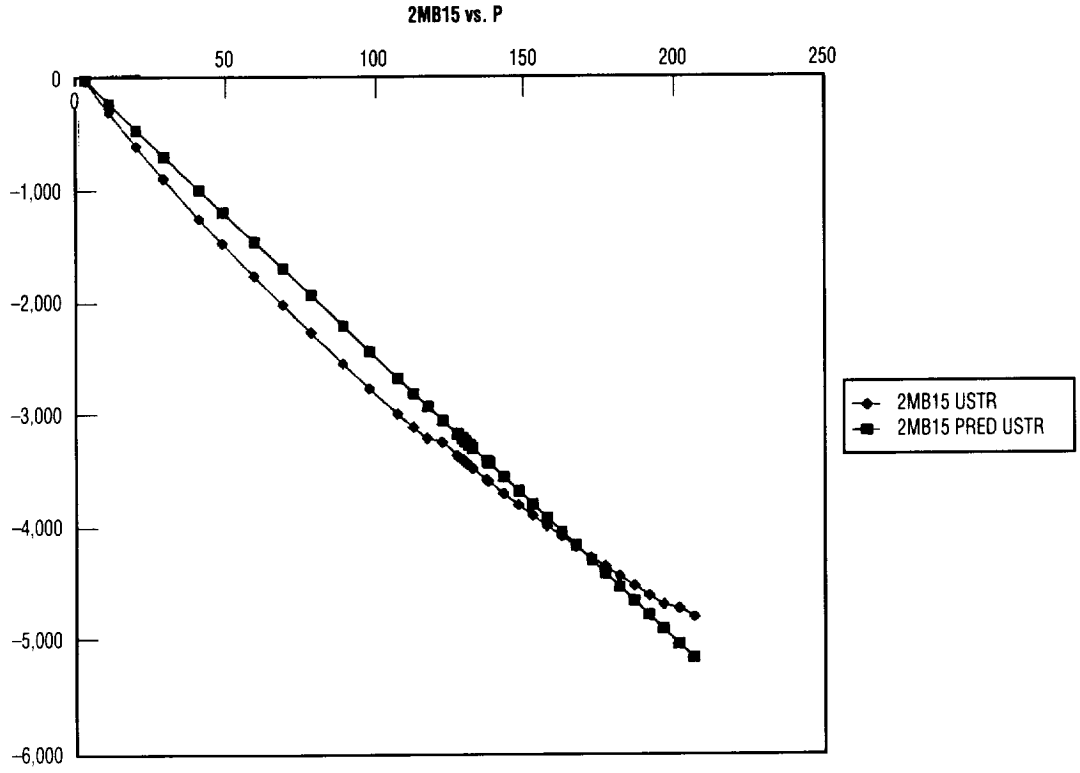

Figure 34. Predicted and actual circumferential strains versus pressure, gauge 2MB15.

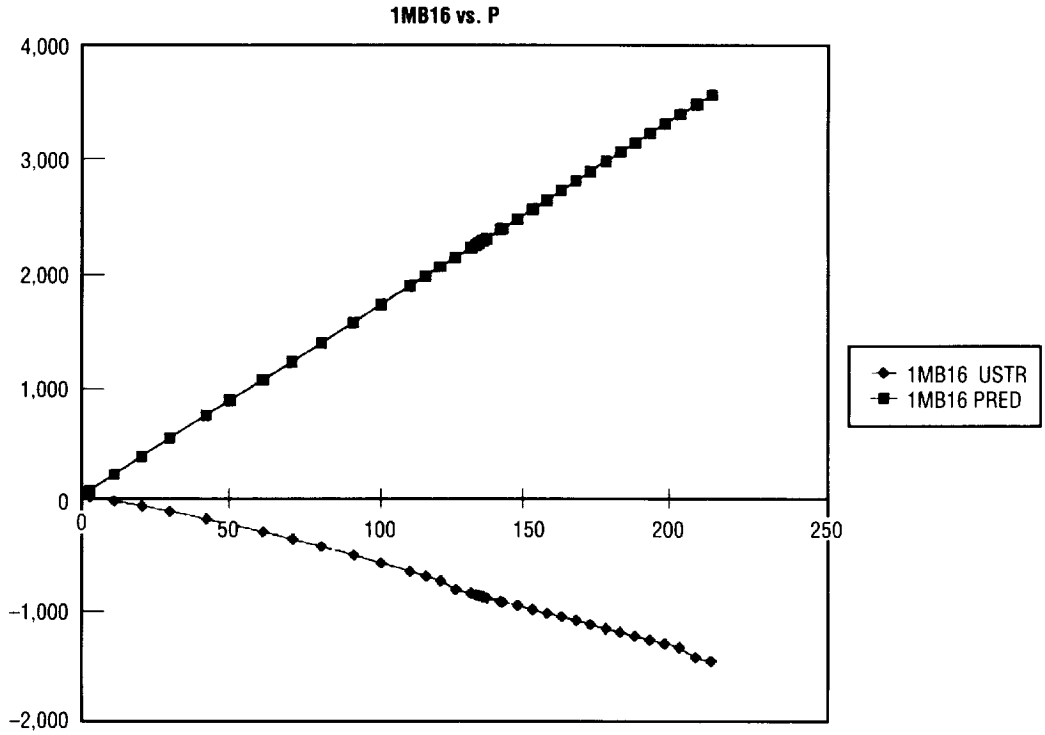

Figure 35. Predicted and actual meridional strains versus pressure, gauge 1MB16.

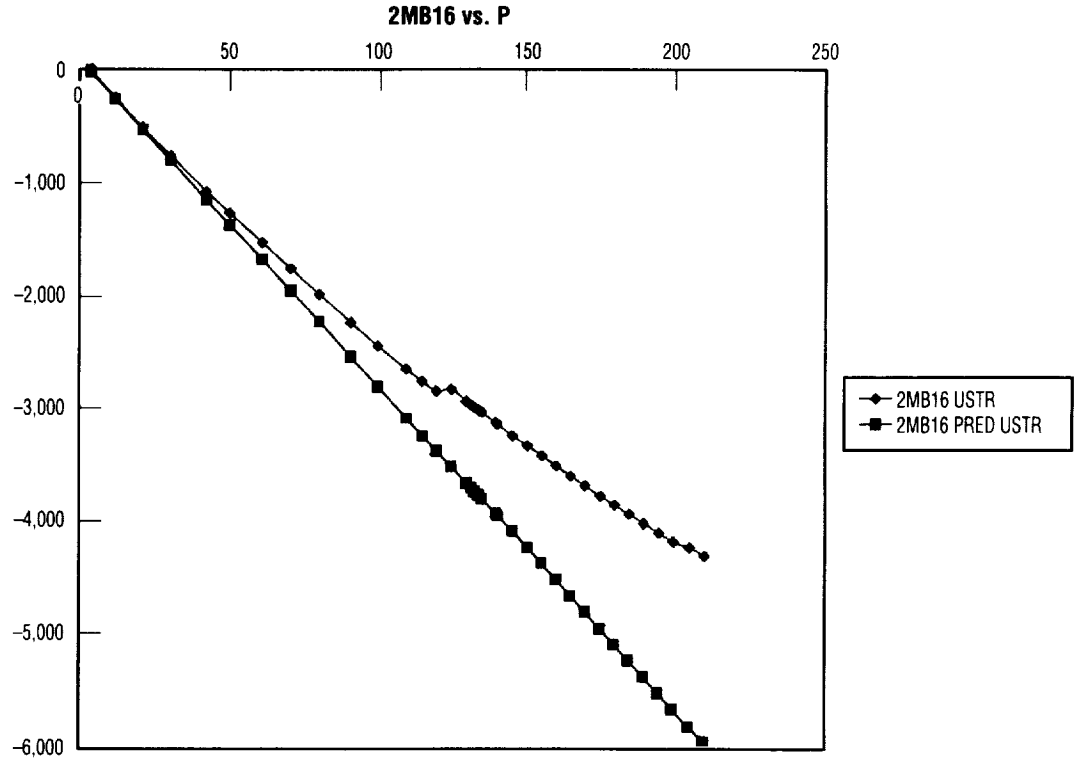

Figure 36. Predicted and actual circumferential strains versus pressure, gauge 2MB16.

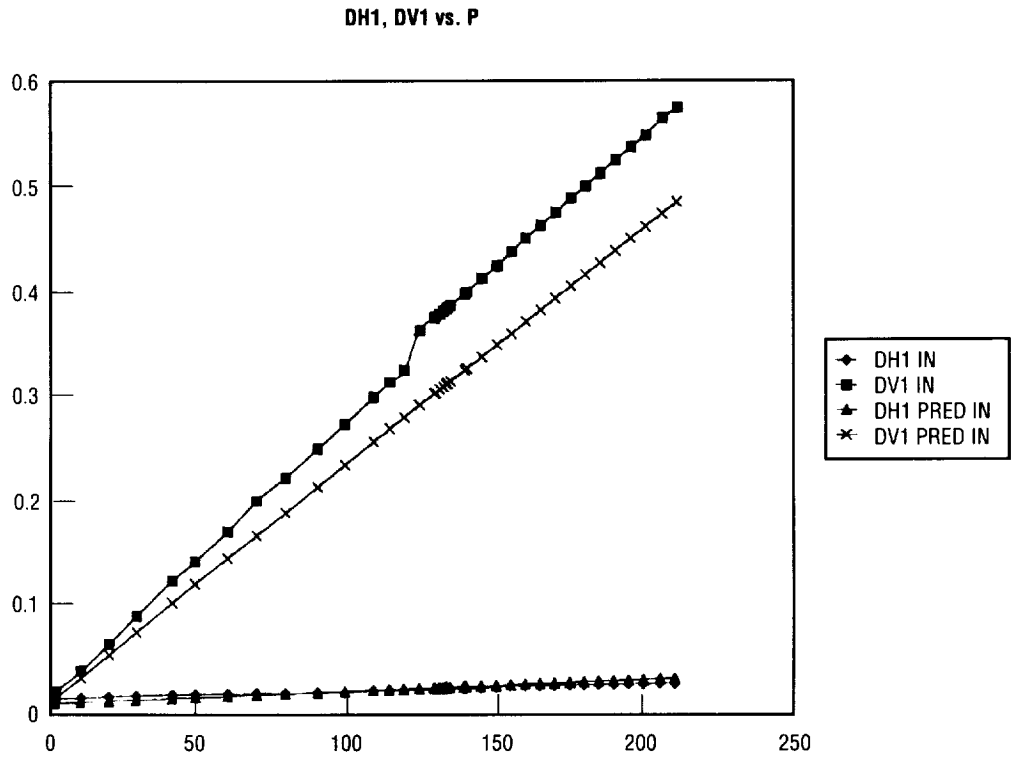

Figure 37. Predicted and actual displacements versus pressure, gauges DH1, DV1.

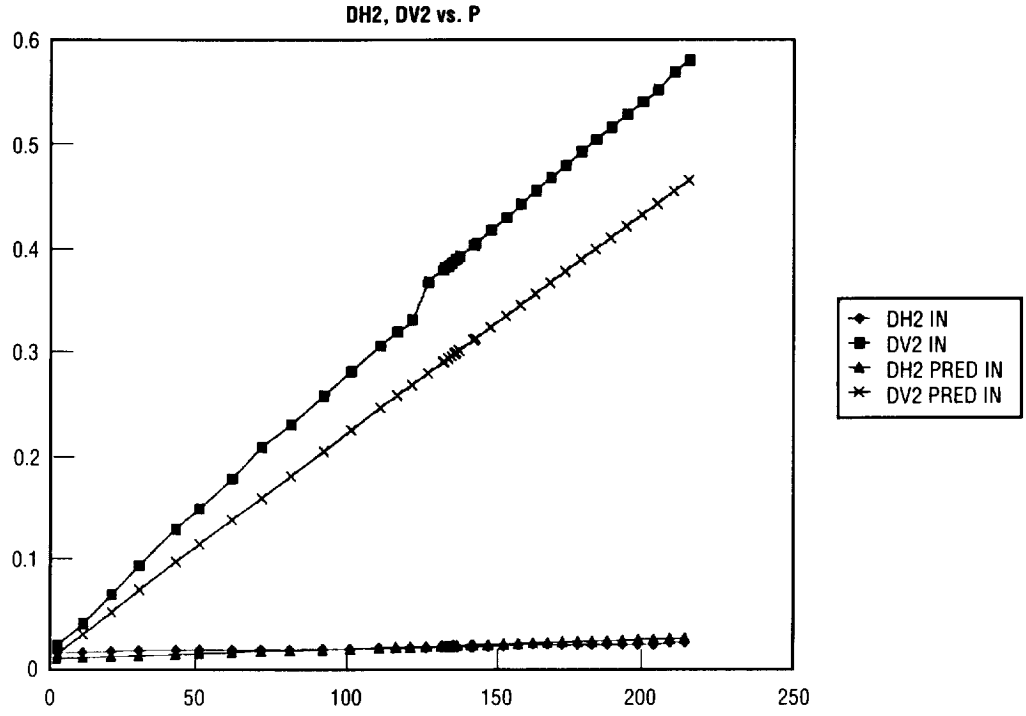

Figure 38. Predicted and actual displacements versus pressure, gauges DH2, DV2.

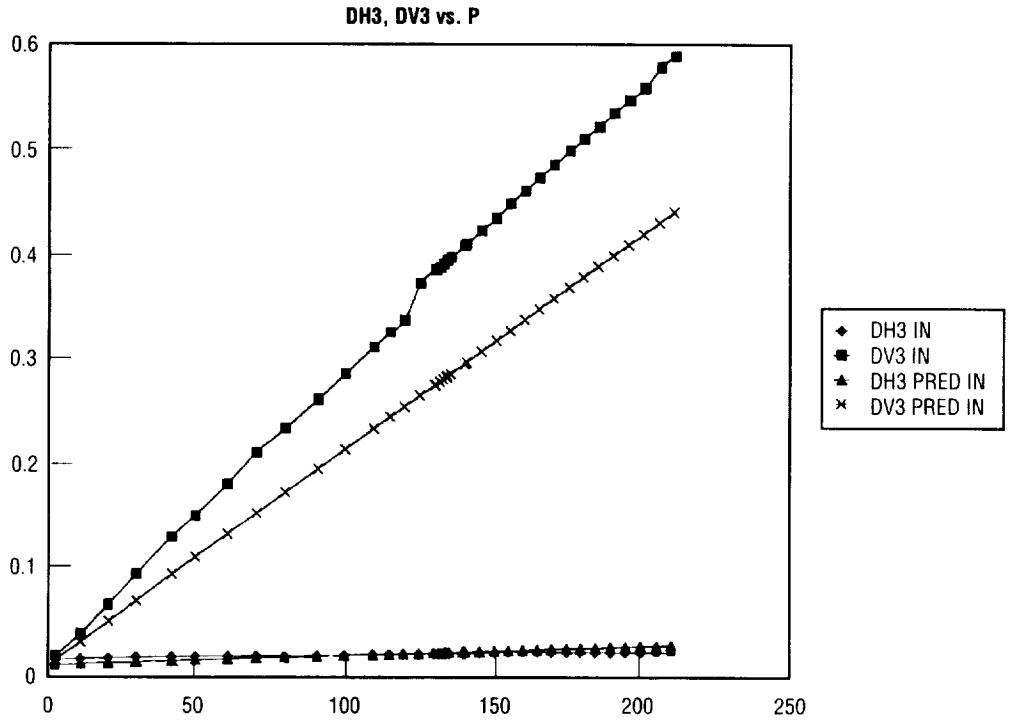

Figure 39. Predicted and actual displacements versus pressure, gauges DH3, DV3.

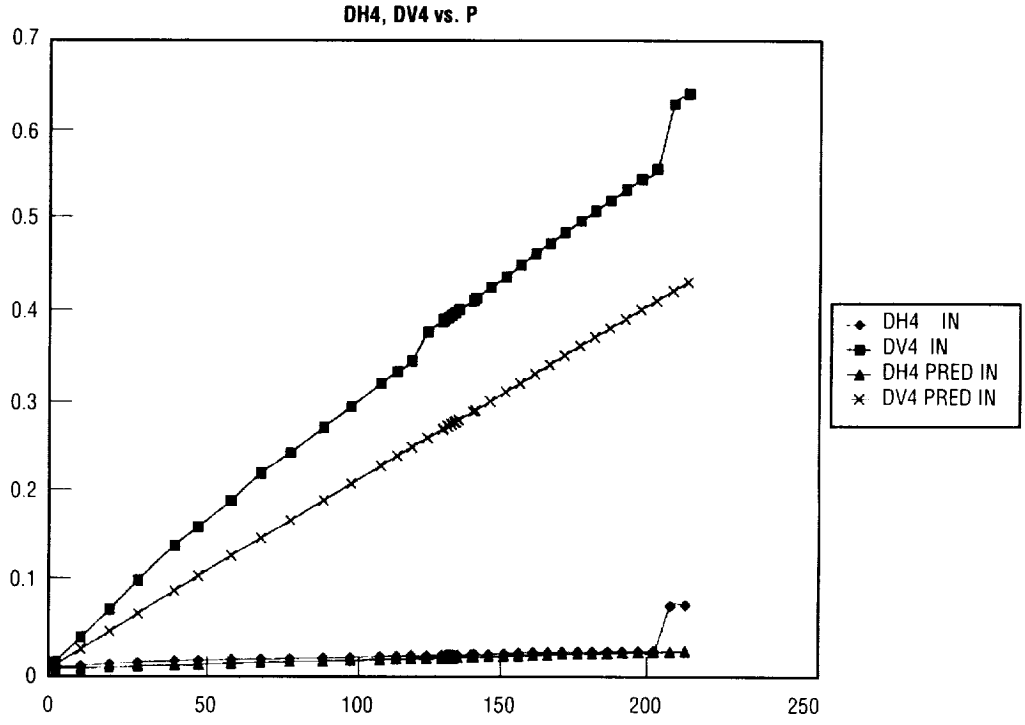

Figure 40. Predicted and actual displacements versus pressure, gauges DH4, DV4.

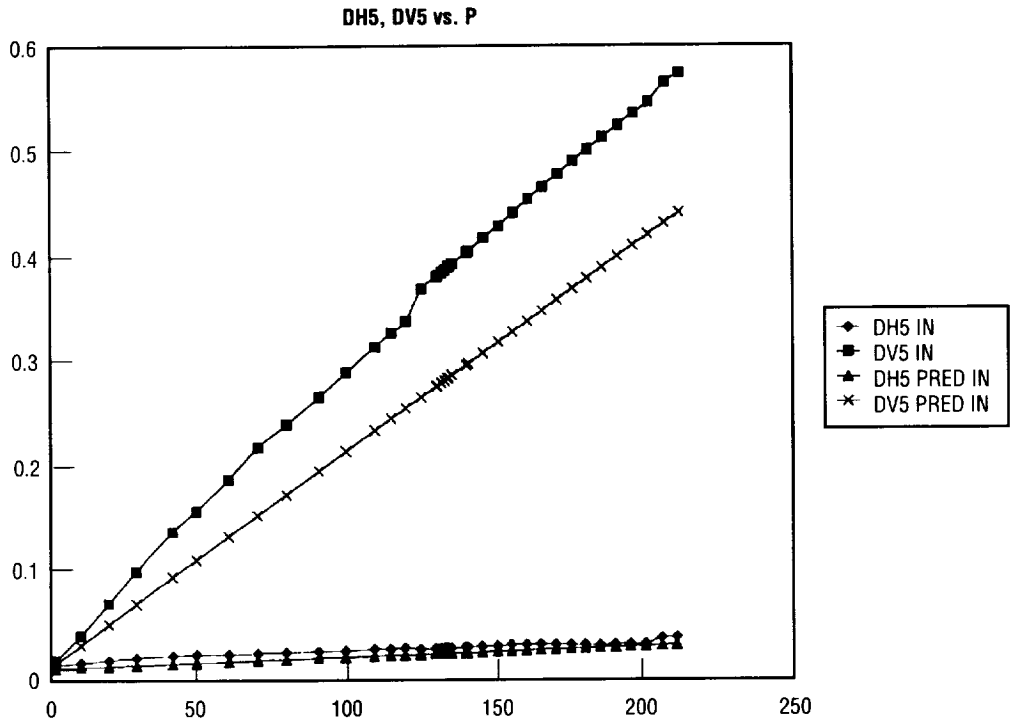

Figure 41. Predicted and actual displacements versus pressure, gauges DH5, DV5.

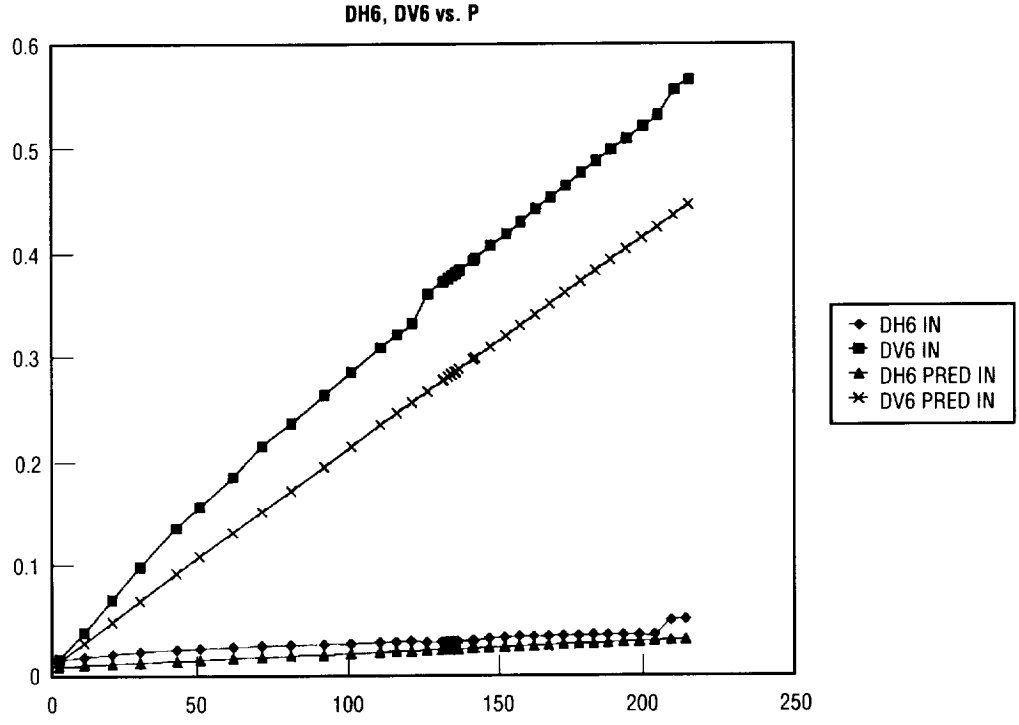

Figure 42. Predicted and actual displacements versus pressure, gauges DH6, DV6.

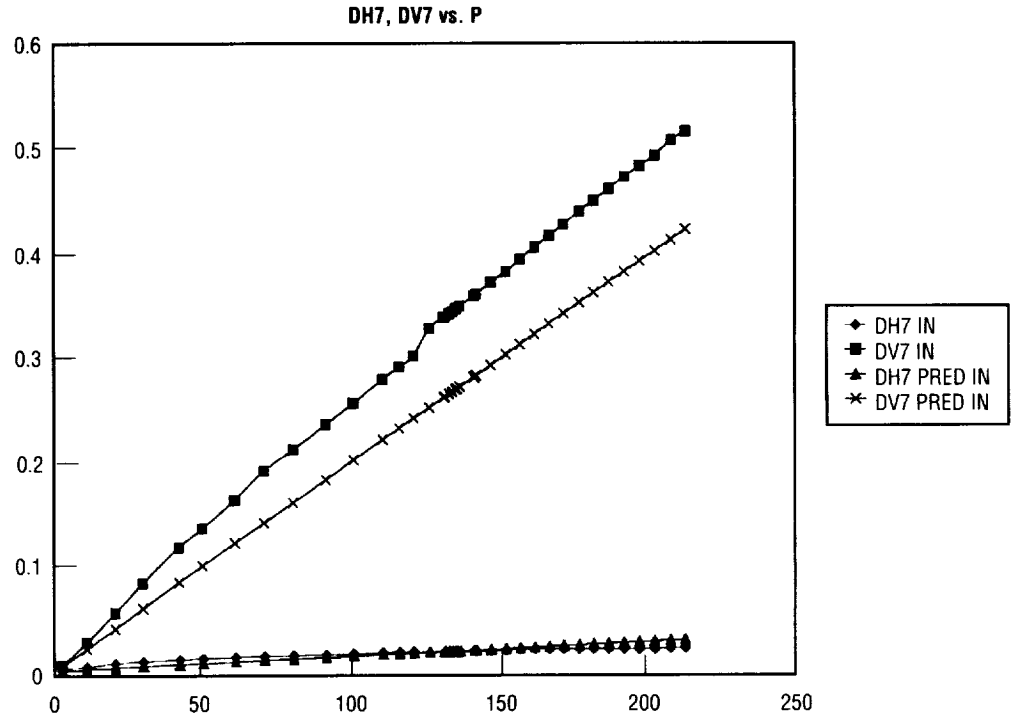

Figure 43. Predicted and actual displacements versus pressure, gauges DH7, DV7.

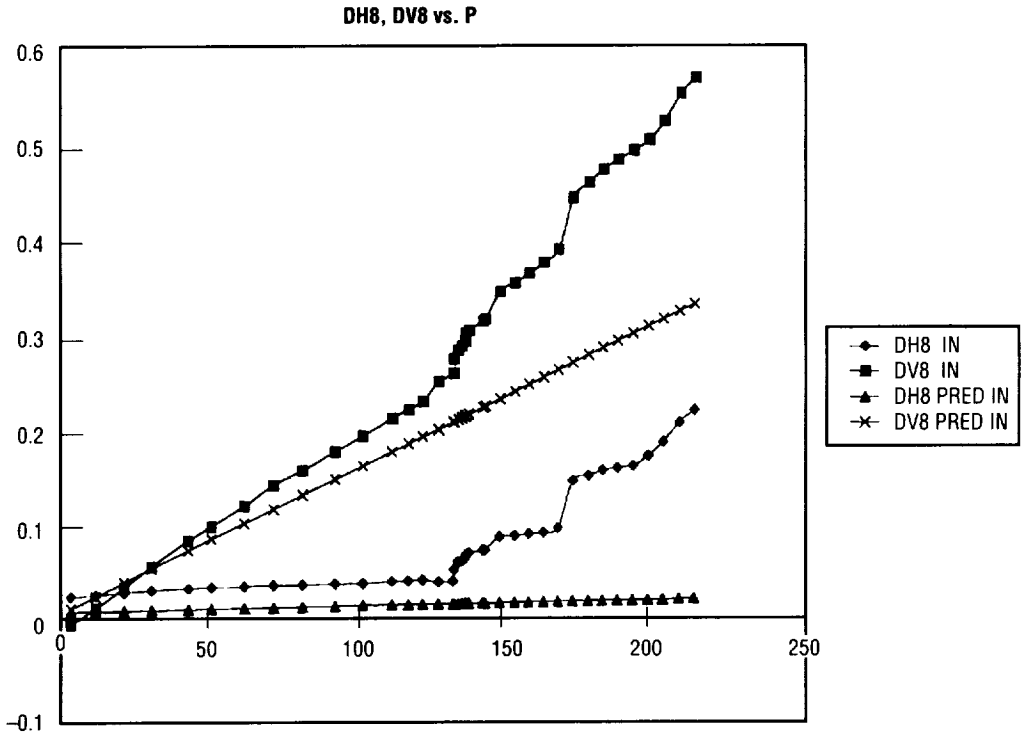

Figure 44. Predicted and actual displacements versus pressure, gauges DH8, DV8.

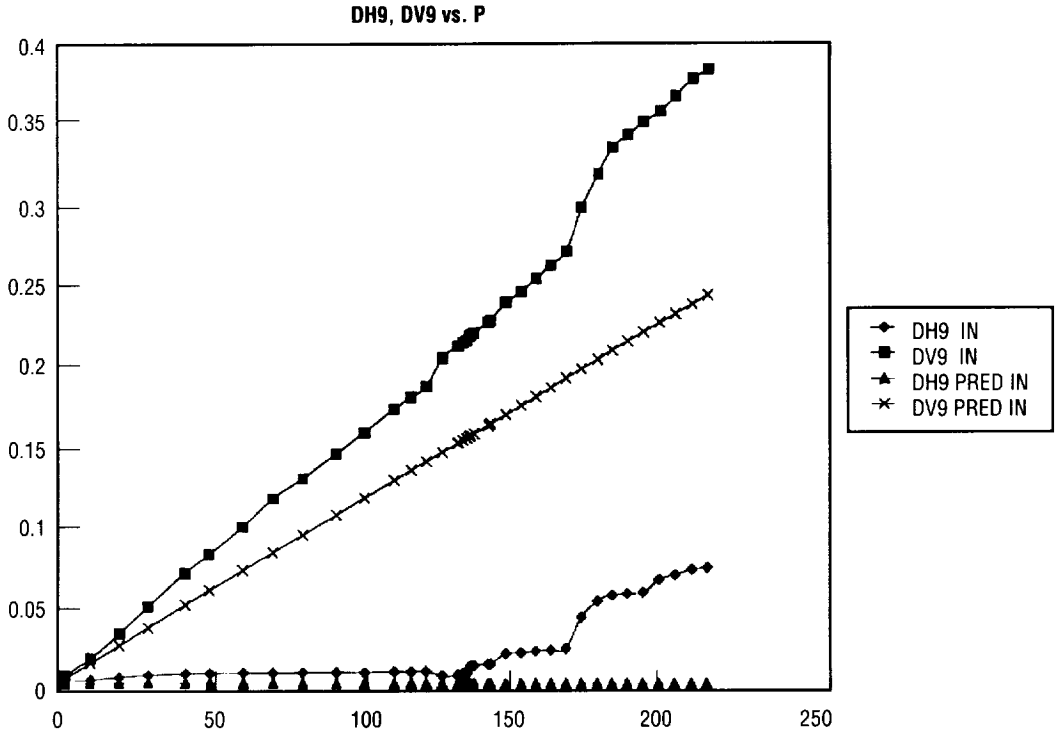

Figure 45. Predicted and actual displacements versus pressure, gauges DH9, DV9.

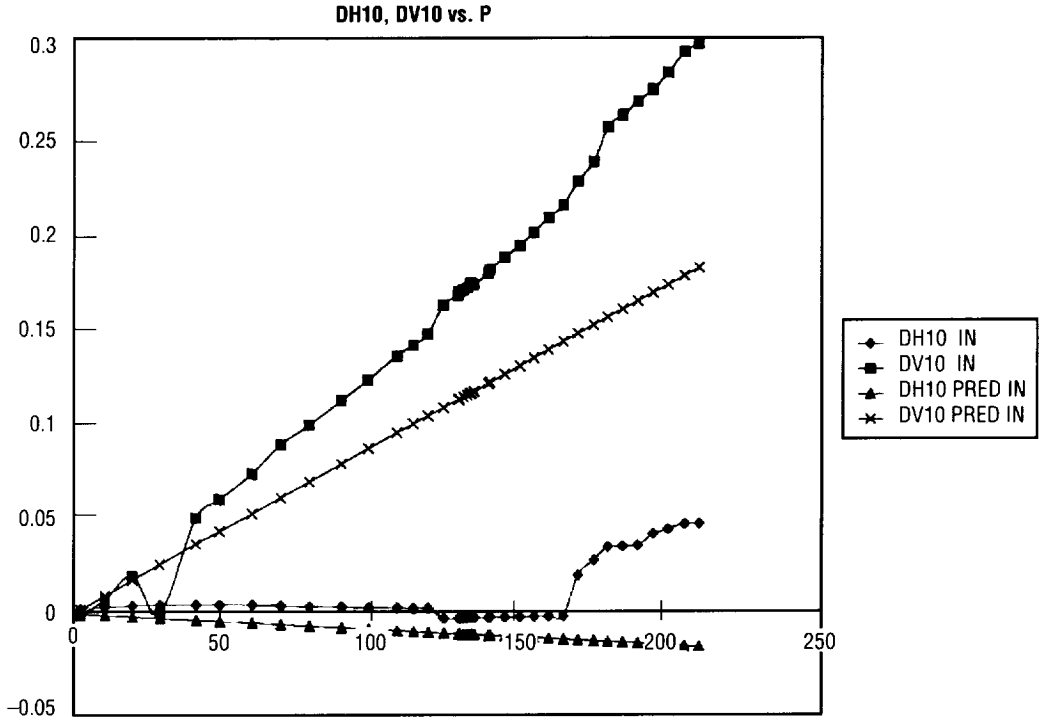

Figure 46. Predicted and actual displacements versus pressure, gauges DH10, DV10.

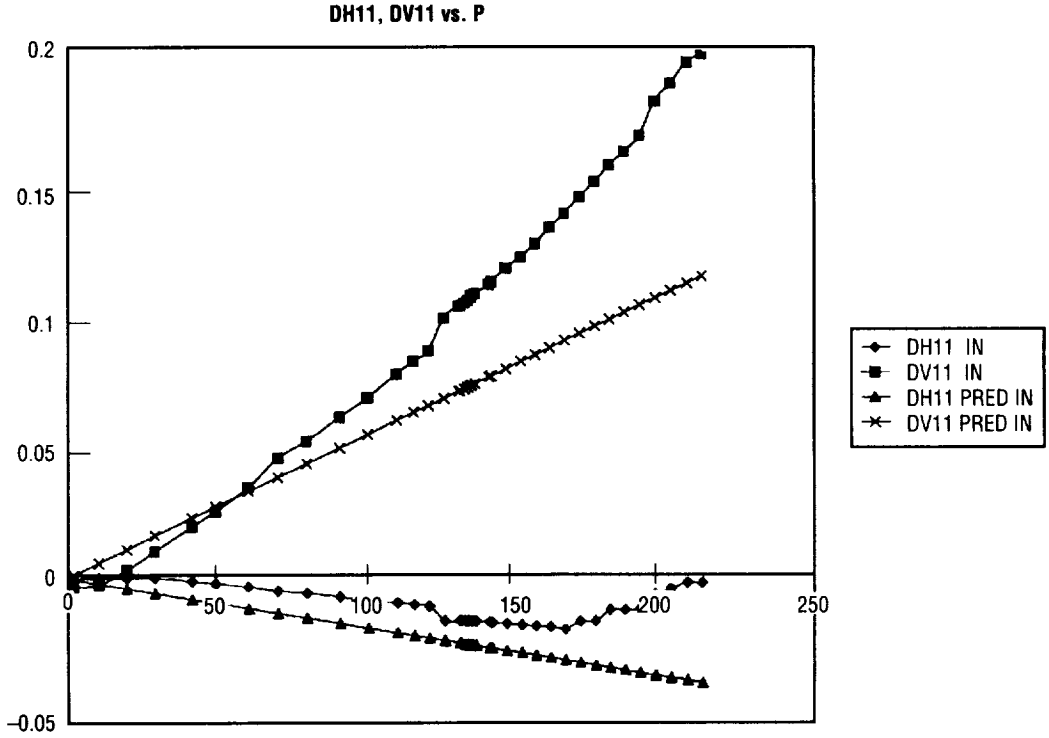

Figure 47. Predicted and actual displacements versus pressure, gauges DH11, DV11.

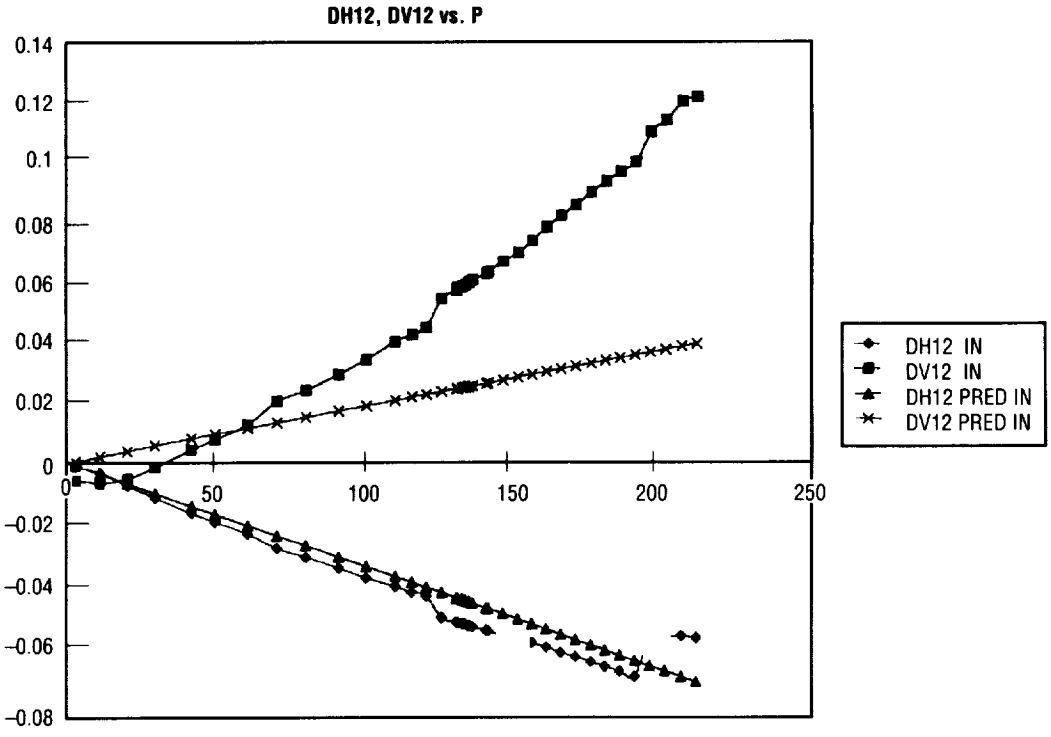

Figure 48. Predicted and actual displacements versus pressure, gauges DH12, DV12.

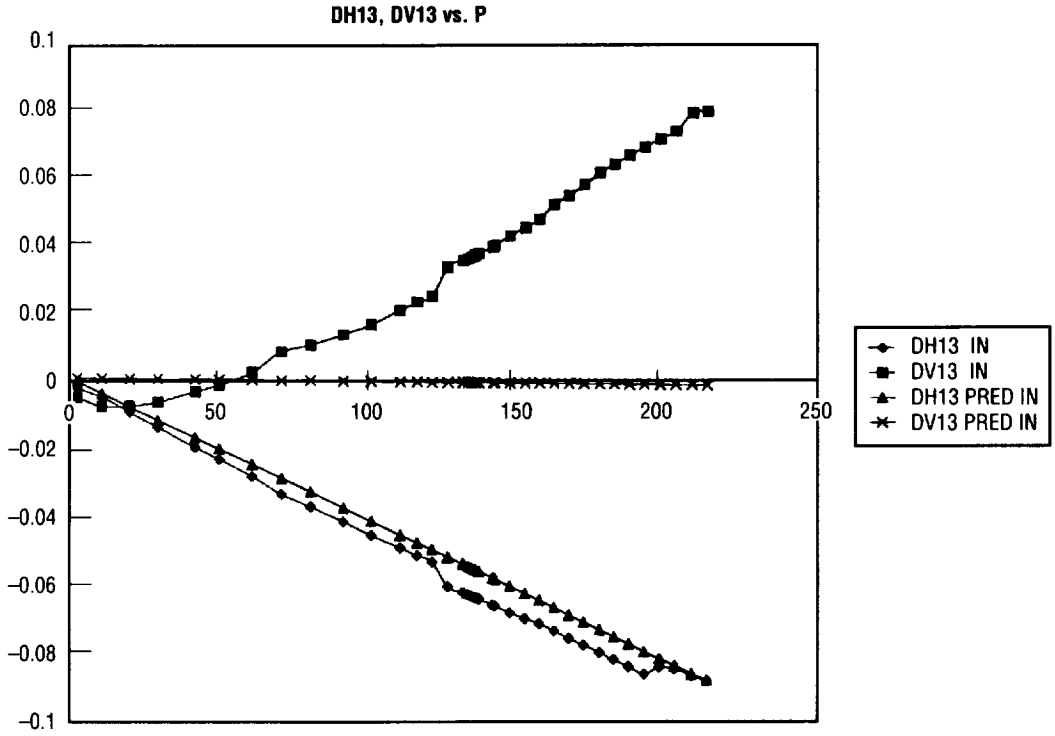

Figure 49. Predicted and actual displacements versus pressure, gauges DH13, DV13.

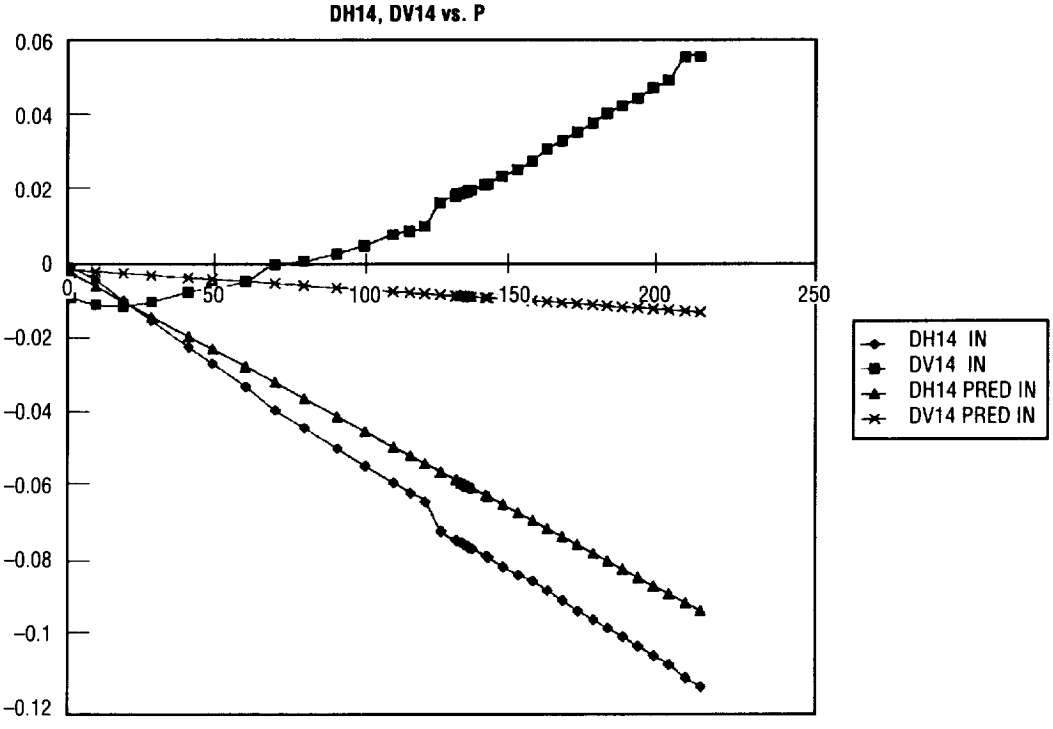

Figure 50. Predicted and actual displacements versus pressure, gauges DH14, DV14.

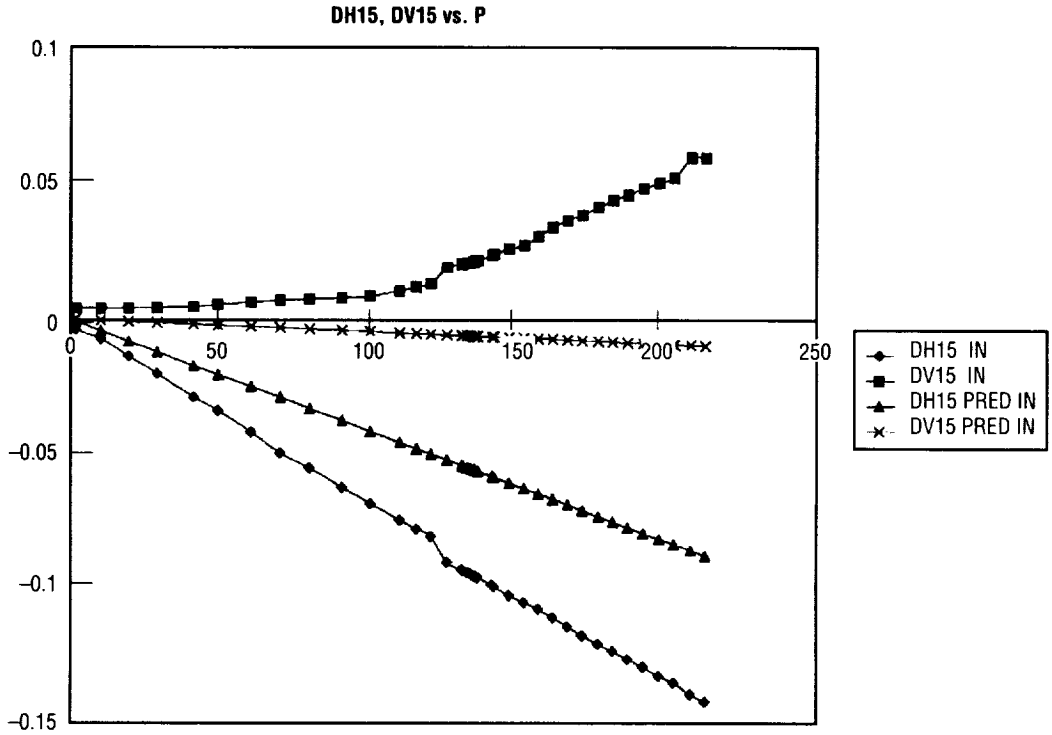

Figure 51. Predicted and actual displacements versus pressure, gauges DH15, DV15.

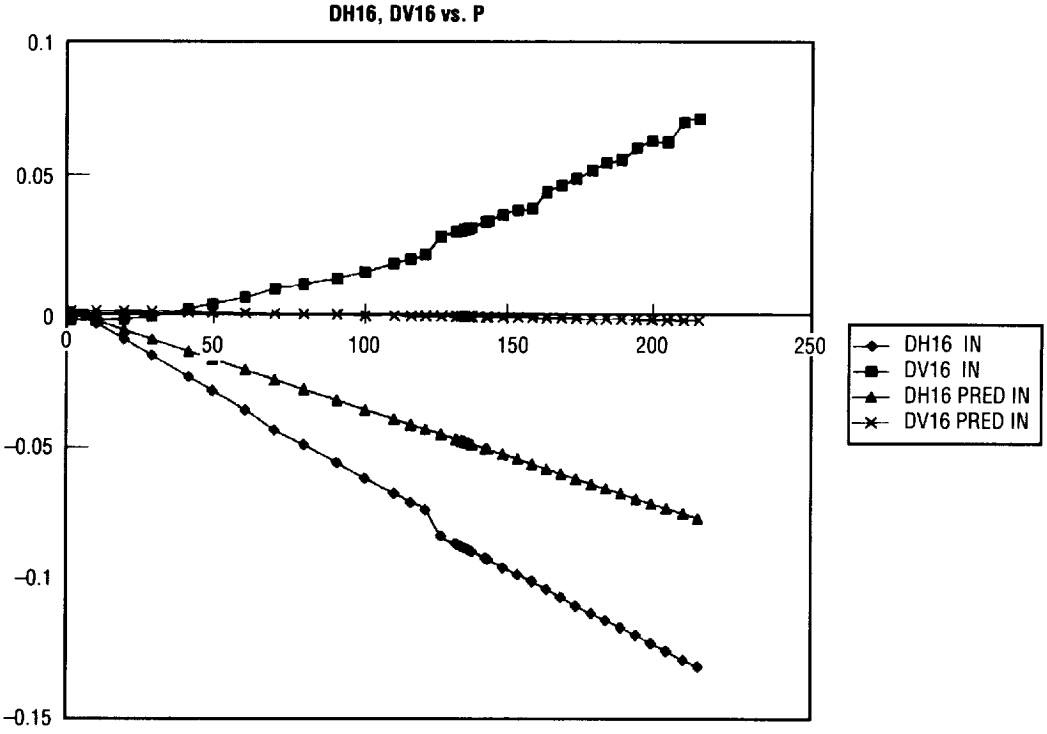

Figure 52. Predicted and actual displacements versus pressure, gauges DH16, DV16.

B. Finite Element Solutions

Since composite laminate theory deals with stresses and strains at a point in the structure, it could not be readily used to determine overall dome displacements. This was accomplished via a 2,820-element, 8,709-node finite element model of the structure using 8-noded elements. The analysis was preprocessed and postprocessed using the PATRAN code and the solution was run using the ANSYS general purpose finite element code.[4] Layups, material properties, and orientations were input into this model and used to calculate the displacements under the internal pressure load. The stresses and strains were also given but were not used in lieu of the analytically obtained results. A plot of the finite element mesh is shown in figure 53.

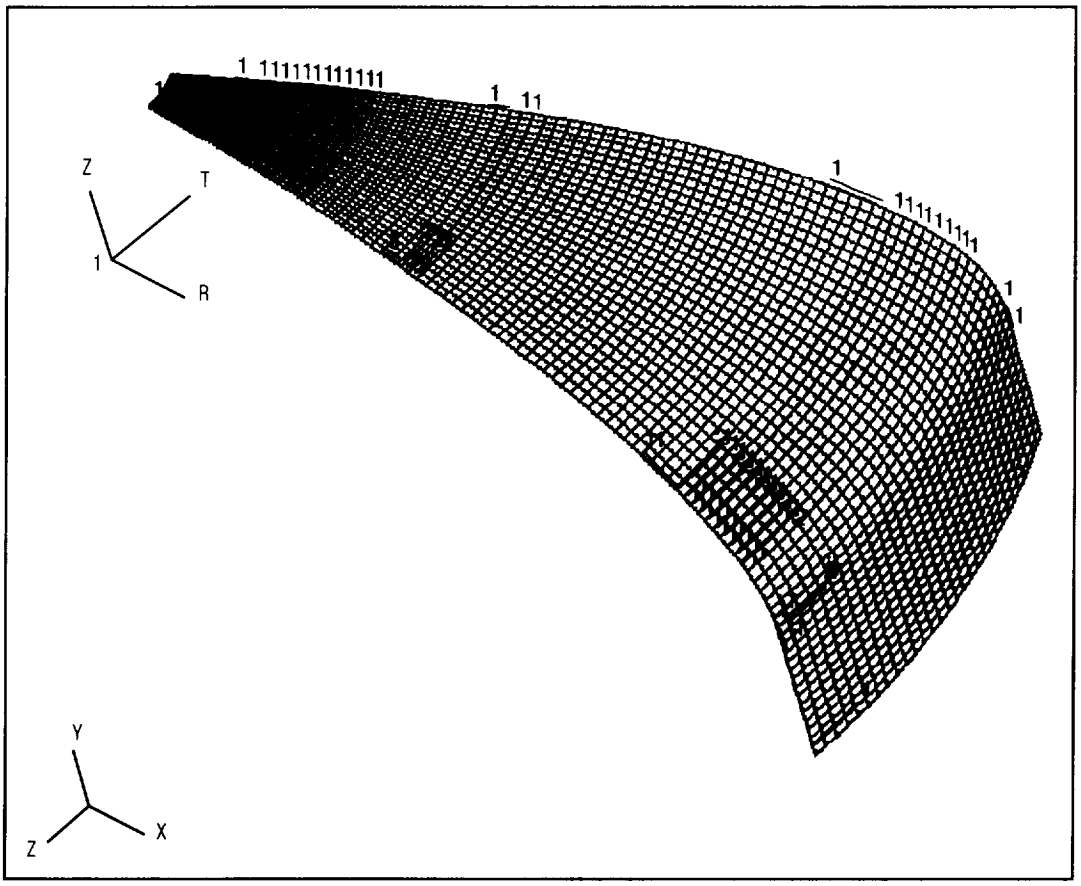

Figure 53. Finite element mesh of low-profile composite dome.

The finite element model was also used to predict the buckling load the dome would experience under the internal pressure loading. The eigenvalue buckling routine in ANSYS was used and the first mode was calculated at 212.89 psi. The typical engineering practice is to employ a knockdown factor for buckling analyses based on empirical data. The only empirical data available to the analyst were from a previous metallic low-profile dome tested at MSFC in 1993. The results from this indicated that a knockdown factor of 0.9 times the first mode buckling eigenvalue was appropriate. Since the dome described here was composite, a more conservative knockdown factor of 0.75 was used to predict first mode buckling. This yielded a predicted first mode buckling at 159.67 psi. The first mode buckling plot given by the analysis is shown in figure 54.

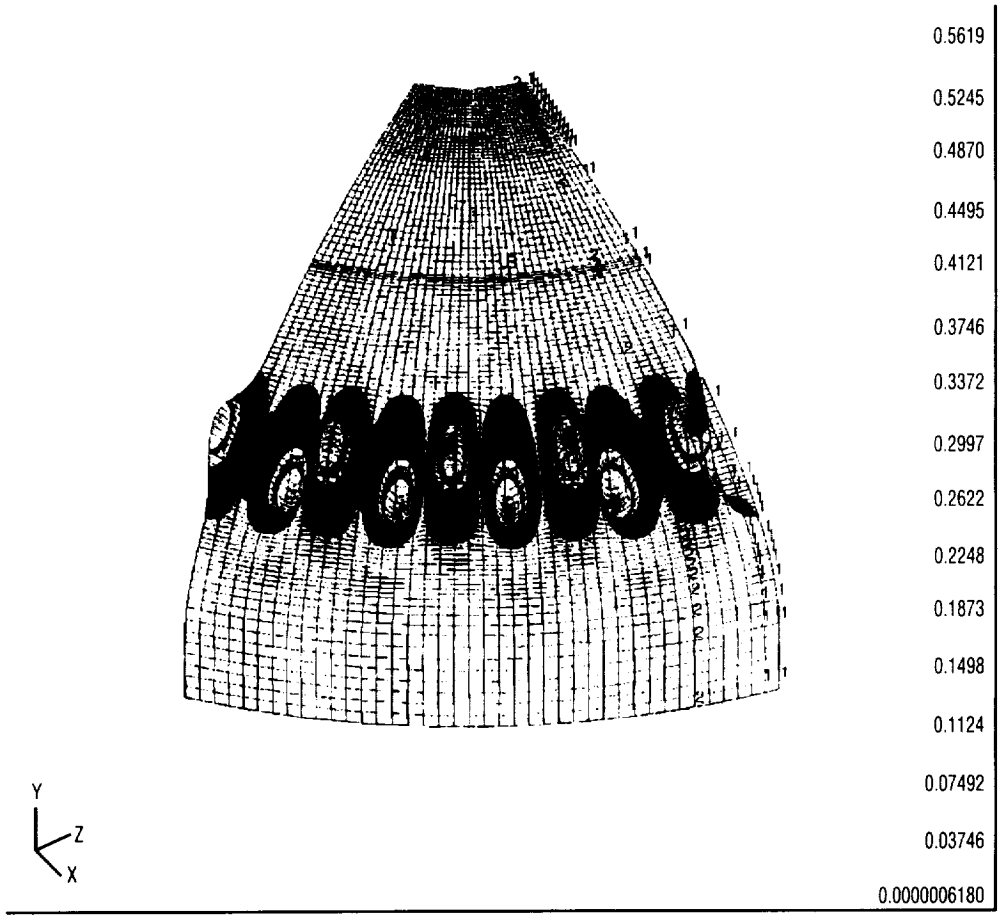

Figure 54. First mode buckling of low-profile composite dome.

IV. TEST

The low-profile composite dome test series was conducted on March 4, 1998, under the supervision of ED71 (MSFC Structural Test Division).

A. Test Article

As mentioned previously, the final test article resulted in a dome about 40.2 in. in diameter and 7 in. high before installation into the test fixture. A 4-in. diameter hole was drilled through the apex center of the dome to accommodate the cover plate, which accommodated the vacuum relief and overflow/ pressure relief valves. Dome thickness varied from 0.25 in. at the equatorial region to 0.06 in. in the mid-latitude regions to 0.3 in. at the apex.

B. Test Fixture Description

The test fixture consisted of three basic components: a cover plate, a base plate, and an interface ring to secure the test article to the base plate.

The base plate was a massive, 3.15-in. thick disk machined out of 2219-T87 aluminum secured by high-strength bolts and clevises to a reaction structure, which, in turn, was bolted to the building floor. A 0.5625-in. diameter drilled and tapped hole was drilled all the way through the base plate disk for water fill and drain. The interface ring consisted of a flanged stainless steel ring with an "L"-shaped axisymmetric cross section with 75 bolt holes to allow bolting to the base plate. The ring section also had 75 bolt holes matching the hole locations of the test article. Both the base plate/interface ring joint and the interface ring/ test article joint incorporated O-rings to insure adequate joint sealing against water leakage during the test. Finally, the cover plate was a 0.5-in. thick disk with 16 blind bolt holes matching those on the test article. To help prevent leakage, it was designed to be installed from inside the test article, thus allowing internal pressure during testing to help the joint sealing. The cover plate/test article joint also incorporated O-rings to insure joint sealing. Plumbing for the vacuum relief and overflow/pressure relief valve systems was run through a 0.75-in. hole and fitting in the cover plate.

C. Test Setup and Pressure Loading

The test setup is shown in figure 55. Water was fed into the dome through a water inlet and then pressurized via missile-grade air to achieve the test pressures.

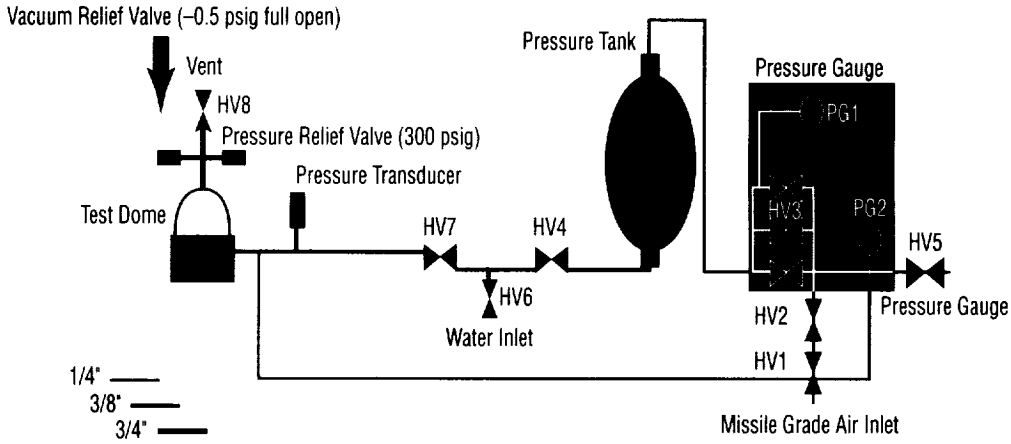

Figure 55. Test setup.

D. Instrumentation

Before the test, the dome was instrumented with strain gauges and electronic displacement indicators (EDI's). Two meridians of strain gauges were located 90° apart circumferentially. A single strip of EDI's was placed at the same radial and meridional coordinates as the strain gauges but on a meridian 45° away and inbetween the strain gauge meridians. This arrangement is shown in the photo in figure 56.

Figure 56. Strain gauge layout.

The strain gauges were identified by an alphanumeric code; e.g., 1MB1. The first number indicated whether the measurement was in the meridonal or hoop direction (1 for meridional, 2 for hoop). The letters "MB" designated a biaxial strain gauge. The second number designated the meridional position of the strain gauge. For the first strip of gauges, this number ranged from 1 (apex of the dome) to 18 (equator of

the dome), and for the second strip, these numbers ranged from 19 (apex) to 36 (equator). The displacement indicators were designated by the letters "DH" (for displacements in the radial direction) or "DV" (for displacements in the vertical direction) followed by a number indicating the meridional position; e.g., DH1 or DV1 (with the number corresponding to the meridional strain gauge location, ranging from 1 at the apex to 18 at the equator). The strain and displacement versus pressure plots presented in this report all use this notation.

In addition to strain gauge and displacement data, acoustic emissions were also employed as a nondestructive evaluation method to determine when failure was imminent (due to ply delaminations, separations, ply failures, or slippage of bolted joints).

E. Test Procedure

A basic summary of the test procedure is outlined below. The loading consisted of the following, in order:

1. Leak check and system checkout up to 25 psi

2. "Influence" test up to 50 psi (to check acoustic emissions, laser and video image equipment)

3. Limit load test to 100 psi

4. Ultimate load test to 140 psi, then continued on to failure of test article.

In each test condition, the pressure was stepped up to 80 percent (to the nearest 10 psi) of the objective in 10-psi increments, then in 5-psi increments the rest of the way. Data scans were taken at every increment along the way and provided to analysts via computer printout. The objective load was held for 5 min and then the load was stepped down in 20-psi increments to zero. Continuous data scanning was maintained during the ramp-down process. Consulting with nondestructive inspection (acoustic emissions, laser and video image correlation) personnel occurred at each increment before proceeding to the next one.

During the test, all gauge readings were stored every 250 msec for influence, limit, and ultimate load tests. After the test was over, all gauge readings were provided in spreadsheet (readable by Microsoft® Excel 5.0) format for each 5 psi of load and every 1 psi after ultimate load has been reached. During the test runs, continuous readouts of strain gauge readings versus load were provided on the data acquisition computer system. In addition, video footage of the test was taken to provide a dynamic replay capability of the test article failure.

Upon completion of the test, the test article was photographed and then disassembled.

F. Results

The dome failure pressure at the end of the ultimate load test was 212 psig, which included the static head pressure of 0.4 psig. No testing anomalies were noted during conduct of the test that would question the validity of any of the posttest data.

V. DISCUSSION

A. Ultimate Failure

The low-profile composite dome ruptured at about 212 psi internal pressure, or 212 percent of the design limit load of 100 psi. The design failure load was 140 percent of design limit, or 140 psi. Based on the different analyses performed, the dome was expected to fail either via circumferential buckling at almost 160 psi or biaxial tension failure at 150 psi, due to the existence of seams in the article. The latter seemed to be the actual failure mode; although the dome did fail at the exact eigenvalue predicted by the analysis, the failure mode did not appear to be that of circumferential buckling. The failure appeared to initiate at the midsection of the dome, where there is a biaxial tension stress state, and cracks progressed simultaneously toward the apex and the equator from this point. There were three crack regions on the dome, each almost 120° apart and running meridionally. One of these three cracks, believed to be the first one that initiated, branched into two cracks, each running toward the equator along lines roughly 120° to the meridional crack. The failed dome is shown in figure 57. At least one of the cracks occurred near a gore seam and could be plainly seen as such. This was an expected failure location, provided the dome did not first buckle.

Figure 57. Low-profile composite dome after failure.

Figure 58. Closeup of one of the failure regions on low-profile composite dome.

B. Displacement and Strain Versus Pressure

The strain results for the test to failure are shown in figures 5 through 36, while the displacement results are shown in figures 39 through 52. Note that results at locations 17 and 18 are not shown since these readings were affected by the additional stiffness of the stainless steel interface ring flange.

Most of the displacement and strain transducers exhibited nonlinear behavior as a function of pressure. This was, in part, due to large deflection and stress stiffening phenomena occurring in the IM7/8552 material as a result of the low thickness regions. This was not accounted for in the analysis since constitutive relations between stress and strain for IM7/8552 in the different material directions were not available.

The strain and displacement behavior for the apex, midsection, and equator regions of the dome are described below. For purposes of discussion, the regions are defined arbitrarily as follows:

- Apex region—radial coordinates ranging from 3.883 to 10.326 in., measured from the dome center

- Midsection region—radial coordinates ranging from 10.326 to 16.963 in., measured from the dome center

- Equator region—radial coordinates ranging from 16.963 to 20.1 in., measured from the dome center.

1. Dome Apex

As a result of using precut gore sections to construct the dome, the ply angles with respect to the curvilinear circumferential and meridional directions were not uniform. That is, the ply angles tended to shift when looking in the circumferential direction. This was particularly true for gores laid near or at the dome apex, where physical dimensions of the gores became larger in comparison to the local radius in the circumferential direction and the local radius in the meridional direction. Naturally, this affected the stress state that occurred in this region and accounted for some difference with respect to the analysis. Circumferential direction stiffnesses were generally lower than predicted by the analysis, although meridional stiffnesses and strain levels tracked the analysis very well.

Axial displacements in this region were generally linear up to about 120 psi (120 percent of limit load), at which there was a slight jump. The cause of this jump was uncertain, but it is seen in all the axial displacement readings and may be due to the onset of slight circumferential buckling at this pressure. Radial displacements, on the other hand, tracked the analysis and were linear with a small magnitude.

2. Dome Midsection

The meridional stress-strain behavior was the most linear in the midsection region of the dome and tracked the analysis well. It was in the circumferential direction that nonlinearities were noted, resulting most likely from the onset of circumferential buckling as the region where hoop compression began was approached. This was also among the thinner regions of the dome, making this area more susceptible to geometric nonlinearity.

Axial displacements were generally linear up to about 120 psi, then became markedly nonlinear after about 130 psi, due to geometric and possibly material nonlinearities. The same was true for the radial displacements. This behavior paralleled similar behavior in the corresponding strain gauges.

3. Dome Equator

In the equator region, the strains exhibited a more linear behavior with respect to stress than in the apex or midsection. Here, the geometric nonlinearities from hoop compression were mitigated by the increased laminate thickness. The stiffnesses in the meridional direction were generally higher than predicted but those in the circumferential direction tracked the analysis quite well.

Axial displacements showed a nonlinear response above 120 to 130 psi, while the radial displacements showed only slight nonlinearity above 130 psi. This was due to the high thicknesses in this region that reduced the stresses and strains.

VI. CONCLUSION

This test program demonstrated that a low-profile dome with a 3-to-1 radius-to-height ratio is feasible with the current composite technology base. The combination of good design practice and the use of handlaid, high-strength graphite cloth material ensured a successful dome that could withstand high pressures and yet have a low weight.

However, manufacturing is an issue as the tested dome had to be constructed via time-consuming hand-layup methods in order to ensure that the required strength was generated. Given the state-of-the-art in filament winding and tape laying at the time of this writing, only cloth with significant strength properties in both orthogonal directions is recommended. Filament-wound or tape-laid low-profile domes would have had lower strength-to-weight ratios compared to handlaid cloth when using the available equipment.

Current design guidelines for low-profile domes derived from this test program are as follows:

1. Cloth material is recommended to maximize strength-to-weight ratio.

2. The equatorial region must be thicker than the midsection of the dome to minimize the tendency for hoop buckling.

3. The apex region of the dome must also be thicker than the midsection to prevent premature biaxial tension failure.

This project paves the way for future investigations in those applications where overall vehicle weight can be reduced by using low-profile domes and also for applications where geometry and space are critical, requiring "flatter" tankage.

REFERENCES

1. Harvey, J.F.: "Theory and Design of Pressure Vessels." Van Nostrand Reinhold, 1980.

2. Garbo, S.P.; and Ogonowski, J.M.: "Effect of Variances on the Design Strength and Life of Mechanically Fastened Composite Joints Volume 3—Bolted Joint Stress Field Model (BJSFM) Computer Program User's Manual." Air Force Wright Aeronautical Laboratories, 1981.

3. Tsai, S.W.; and Hahn, T.H.: "Introduction to Composite Materials." Technomic, 1980.

4. "ANSYS User's Manual." ANSYS, Inc., 1995.

REPORT DOCUMENTATION PAGE

Form Approved
OMB No. 0704-0188

Public reporting burden for this collection of information is estimated to average 1 hour per response, including the time for reviewing instructions, searching existing data sources, gathering and maintaining the data needed, and completing and reviewing the collection of information. Send comments regarding this burden estimate or any other aspect of this collection of information, including suggestions for reducing this burden, to Washington Headquarters Services, Directorate for Information Operation and Reports, 1215 Jefferson Davis Highway, Suite 1204, Arlington, VA 22202-4302, and to the Office of Management and Budget, Paperwork Reduction Project (0704-0188), Washington, DC 20503

1. AGENCY USE ONLY *(Leave Blank)*	2. REPORT DATE	3. REPORT TYPE AND DATES COVERED
	May 1999	Technical Publication

4. TITLE AND SUBTITLE
Design and Test of Low-Profile Composite Aerospace Tank Dome
(MSFC Center Director's Discretionary Fund Final Report, Project No. 96-28)

5. FUNDING NUMBERS

6. AUTHORS
R. Ahmed

7. PERFORMING ORGANIZATION NAMES(S) AND ADDRESS(ES)
George C. Marshall Space Flight Center
Marshall Space Flight Center, Alabama 35812

8. PERFORMING ORGANIZATION REPORT NUMBER
M–928

9. SPONSORING/MONITORING AGENCY NAME(S) AND ADDRESS(ES)
National Aeronautics and Space Administration
Washington, DC 20546–0001

10. SPONSORING/MONITORING AGENCY REPORT NUMBER
NASA/TP—1999–209267

11. SUPPLEMENTARY NOTES
Prepared by Structures and Dynamics Laboratory, Science and Engineering Directorate

12a. DISTRIBUTION/AVAILABILITY STATEMENT
Unclassified–Unlimited
Subject Category 39
Standard Distribution

12b. DISTRIBUTION CODE

13. ABSTRACT *(Maximum 200 words)*

This report summarizes the design, analysis, manufacture, and test of a subscale, low-profile composite aerospace dome under internal pressure. A low-profile dome has a radius-to-height ratio greater than the square root of two. This effort demonstrated that a low-profile composite dome with a radius-to-height ratio of three was a feasible design and could adequately withstand the varying stress states resulting from internal pressurization. Test data for strain and displacement versus pressure are provided to validate the design.

14. SUBJECT TERMS
composites, graphite epoxy, tanks, domes, internal pressure, low profile, bulkheads, optimization

15. NUMBER OF PAGES
56

16. PRICE CODE
A04

17. SECURITY CLASSIFICATION OF REPORT	18. SECURITY CLASSIFICATION OF THIS PAGE	19. SECURITY CLASSIFICATION OF ABSTRACT	20. LIMITATION OF ABSTRACT
Unclassified	Unclassified	Unclassified	Unlimited